Hydrol. Earth Syst. Sci., 30, 7197–7224, 2026
https://doi.org/10.5194/hess-30-7197-2026
© Author(s) 2026. This work is distributed under
the Creative Commons Attribution 4.0 License.

Hydrology and Earth System Sciences
Open Access
EGU

New insights from fully-integrated surface-subsurface hydrological modeling in high-elevation glaciated environments

Xinyang Fan[1,2], **Florentin Hofmeister**[3,4], **Bettina Schaefli**[1], **and Gabriele Chiogna**[2]

[1]Institute of Geography and Oeschger Centre for Climate Change Research, University of Bern, Bern, Switzerland
[2]Department of Geography and Geosciences, GeoZentrum Nordbayern, Friedrich-Alexander-University Erlangen-Nuremberg, Erlangen, Germany
[3]Chair of Hydrology and River Basin Management, School of Engineering and Design, Technical University of Munich, Munich, Germany
[4]Bavarian Academy of Sciences and Humanities, Munich, Germany

Correspondence: Xinyang Fan (xinyang.fan@unibe.ch)

Received: 5 December 2025 – Discussion started: 11 December 2025
Revised: 23 September 2026 – Accepted: 14 November 2026 – Published: 23 November 2026

Abstract. Recent modeling efforts go towards distributed physics-based modeling for improved hydrological process understanding. The sparse hydro-meteorological observations and complex topography in high-elevation mountainous environments have, however, hampered the application of such data-intensive and sophisticated techniques for detailed process exploration. In particular, characterizing surface-subsurface water exchange processes in these terrains remains understudied. Here we implement a fully-integrated and fully-distributed surface-subsurface hydrological model, *WaSiM*, to quantify the observed daily streamflow variations and their interactions with groundwater in the high-elevation glaciated catchment (Martell Valley) in the central European Alps since the 2000s. Extensive field observations (meteorology, vegetation, glacier mass balance, soil properties, river discharge), especially in-situ groundwater levels, were collected to investigate hydrological processes and constrain model parameters in the surface and subsurface. We observe that in contrast to the delayed responses typically observed in aquifers, shallow alpine groundwater responds nearly as quickly as streamflow to peak snowmelt and extreme rainfall events, highlighting the need for improved subsurface parametrization in hydrological modeling. Joint evaluation against shallow groundwater heads and streamflow shows that the daily streamflow and shallow groundwater dynamics can be reproduced without requiring the *WaSiM* interflow component, providing new constraints on the representation of unsaturated-zone flow pathways in high Alpine hydrological models. Moreover, to improve the integration of point-scale groundwater observations into fully-distributed models, we suggest pre-calculating the Topographic Wetness Index to stratify hydro-topographic settings and combining this information with other site characteristics to guide piezometer placement. Despite uncertainties associated with model structure and subsurface representation, this study demonstrates the value of groundwater observations for constraining internal flow partitioning in hydrological modeling.

1 Introduction

With rising temperatures and increasing frequency and intensity of hydrological extremes, many regions worldwide are experiencing severe impacts of climate change (IPCC, 2021). Mountain glaciers are among the most sensitive indicators of climate change, with widespread glacier retreat and declining snowfall observed globally (Rounce et al., 2023; Matiu et al., 2021; Marcolini et al., 2017). These changes threaten downstream water availability, hydropower production, and ecosystem functioning, while increasing risks associated with glacier-related hazards such as glacial lake outburst floods (Banerjee et al., 2024; Drenkhan et al., 2023; Wechsler et al., 2023). Therefore, improving our understanding of hydrological processes and water storage changes in high-elevation environments is essential for projecting future

water resource availability and associated societal impacts (van Tiel et al., 2024).

Hydrological models have been widely used to assess climate change impacts on alpine water resources. Many applications rely on lumped-parameter or semi-distributed models, such as HBV, mHM, THREW-T, and T&C (Seibert and Bergström, 2022; Nan et al., 2021; Kumar et al., 2013; Fatichi et al., 2012). These models have successfully reproduced catchment-scale runoff responses but generally represent subsurface processes using simplified conceptual approaches, such as one-dimensional linear reservoirs or direct drainage from soil layers to streams without a groundwater module (Coderre et al., 2026; Horton et al., 2022). Consequently, groundwater storage, recharge, and baseflow generation are often poorly represented, introducing uncertainties in projections of future hydrological changes (Puspitarini et al., 2020; Tuo et al., 2018). In particular, streamflow simulations in high Alpine catchments frequently show deficiencies in representing winter baseflow and the timing of melt-driven runoff increases (Michel et al., 2022; Schaefli et al., 2014; Schaefli and Huss, 2011).

Improving streamflow simulations in mountain environments has traditionally focused on improving snow representation, as errors in snow distribution and melt timing are commonly considered major sources of uncertainty (Freudiger et al., 2017; Warscher et al., 2013; Dobler and Pappenberger, 2013). However, recent evaluations suggest that many snow models can reproduce observed snow dynamics reasonably well (Hofmeister et al., 2022; Carletti et al., 2022; Schlögl et al., 2016). This indicates that deficiencies in alpine hydrological simulations may also originate from missing processes or oversimplified model structures, particularly the representation of groundwater and surface-subsurface interactions (Somers and McKenzie, 2020). Despite the recognized importance of groundwater in regulating streamflow variability, its role in high Alpine hydrological systems remains poorly constrained. Groundwater observations are often the most limited in high-elevation glaciated environments, making them one of the least available but most valuable data sources for evaluating integrated hydrological models (Borzi, 2025; Fan et al., 2023a; Hofmeister et al., 2023a).

Quantifying groundwater-surface water interactions remains challenging in mountainous regions due to complex topography, geology, and coupled surface–subsurface processes, with additional complexities introduced by snow and glacier melt in cryosphere-dominated environments (Abhervé et al., 2023; Fan et al., 2023b; Krause et al., 2007). Accordingly, the widely accepted runoff-generation classification by Dunne (1983) indicates that, in humid climates and steep terrain, runoff generation is commonly dominated by lateral subsurface stormflow in combination with saturation-excess overland flow (Trancoso et al., 2016). However, streamflow generation processes in steep cryospheric terrain remain poorly understood, and the applicability of the Dunne diagram to such environments remains uncertain (Trancoso et al., 2016; Dunne, 1983). Recent studies investigated groundwater storage, geological controls on groundwater dynamics, and physically based representations of surface-subsurface interactions in Alpine catchments (Müller et al., 2024; Engdahl, 2024; Thornton et al., 2022; Arnoux et al., 2021; Somers et al., 2016). However, the challenges remain: semi-distributed models lack sufficient spatial resolution to capture heterogeneous groundwater responses (Chen et al., 2023), whereas fully distributed approaches require detailed hydrogeological information and are challenging to apply due to sophisticated model structure, parameterization, and calibration (Thornton et al., 2022; Engdahl, 2024).

A handful of studies have applied integrated surface-subsurface hydrological models in cryosphere-dominated Alpine catchments. Thornton et al. (2022) coupled *WaSiM* (Schulla, 2024, 1997) with *HydroGeoSphere* (Aquanty, 2016) to investigate groundwater-cryosphere interactions and highlighted the importance of near-surface processes in regulating meltwater and rainfall partitioning between surface and subsurface pathways. More recently, Aubry-Wake et al. (2024) applied a fully-integrated hydrological response unit (HRU)-based framework – *Cold Regions Hydrological Modelling Platform* (Pomeroy et al., 2007) to investigate cryosphere-surface water-groundwater interactions, but the contributions of overland flow and subsurface lateral flow to streamflow are not quantified separately, while van Tiel et al. (2024) emphasized the broader challenges of representing groundwater processes in glaciated environments.

To contribute to overcoming these challenges, this study presents one of the first applications of a fully-distributed and fully-integrated surface–subsurface hydrological modeling approach in the high-elevation glaciated environment. The *WaSiM* model (Schulla, 2024, 1997) is adopted, given that it is one of the very few fully-distributed and fully-integrated hydrological models suitable for modeling high-elevation glaciated environments. By explicitly representing unsaturated-zone and groundwater flow processes and constraining the model with extensive hydro-meteorological observations, including rare in-situ groundwater level measurements, we investigate surface and near subsurface hydrological processes and storage dynamics in the Martell Valley (Northern Italy). Beyond evaluating model performance, this study aims to assess what new insights can be obtained from an integrated modeling framework regarding water partitioning between the surface and subsurface domains, while also identifying the limitations and practical challenges associated with applying such models in data-scarce mountain regions.

Specifically, this study addresses the following questions: (i) Can a fully-distributed and fully-integrated hydrological model reproduce both streamflow and shallow groundwater dynamics in a high-elevation glaciated catchment? (ii) What new insights into surface-subsurface water exchange and hydrological processes can be achieved from such a detailed modeling framework? (iii) What are the opportunities and

limitations of applying fully-distributed and fully-integrated hydrological models under the observational data constraints typical of high Alpine environments?

2 Study site

The Martell Valley is a high-elevation glaciated catchment in the central European Alps (Northern Italy, see Fig. 1a, b) with an elevation range of 1777 to 3743 m a.s.l (mean: 2737 m a.s.l.) and fine-scale topography. The catchment has an area of 77 km^2 including 9 subcatchments (S1–S9) and it is closed at the Zufritt Lake. It is covered by around 34 % of grassland (growing upon shallow soil formation), 9 % of forests, 17 % of glaciers, and 40 % area of exposed rocks and soil (CORINE Land Cover, 2018) (Fig. 1c). The glaciers are mainly located in the southwest of the catchment, with the largest being Langenferner, Zufallferner, and Fürkeleferner. These glaciers reached their largest extension during the last Little Ice Age (LIA). Glacier retreat has been observed since the 1850s and accelerated since the 1980s (Knoflach et al., 2021). It is one of the key drivers of high Alpine geosystem changes, such as land cover, ecological succession, hydrology, and geomorphology (Ramskogler et al., 2023; Knoflach et al., 2021).

We derive the catchment hydrogeology information based on the dominant geological characteristics available in the geology map and geodatabase (Fig. 1a) (Ramskogler et al., 2023; Berra et al., 2012). In the mapping area (except Subcatchment S1 due to lack of data), the rock units take 35 % (likely presence of fractured and fissured aquifers) and the sedimentary units take 45 % (likely presence of porous aquifers); the rest of the information under the glacier is unavailable. The dominant rock units are orthogneiss, phyllite, quartz, and marble (Ramskogler et al., 2023; Berra et al., 2012). Climatically, this catchment is relatively dry among the European Alps (Höge et al., 2023; Ceperley et al., 2020; Isotta et al., 2018). It has a mean annual temperature of −1.2 °C between 2007 and 2023, with the maximum of 0.2 °C in 2022 and the minimum of −2.9 °C in 2010 (based on the interpolated catchment mean, Sect. 3.1). The mean annual precipitation and modeled evapotranspiration (Sect. 3.1) are 1048 and 167 mm yr^{-1} for the same period. 2014 is the wettest year, with the highest annual precipitation of 1368 mm and the lowest evapotranspiration of 122 mm. 2022 is the driest year, with the lowest annual precipitation of 661 mm and the highest annual evapotranspiration of 218 mm.

Most of the hydro(geo)logical stations are located in the upper Subcatchments S7–S9, which comprise a proglacial outwash plain in the form of an alluvial fan (Fig. 1). As the majority of the stations are located in this area, our primary study focus is on these subcatchments, with the model calibrated to the observations from this region. However, the modeling results are presented both for the upper subcatchments in detail (with higher confidence) and for the entire catchment to provide an overview (with lower confidence). This decision is motivated by the fact that prior studies in Martell Valley are interested in the streamflow in both upper subcatchments and at the catchment outlet (Schaffhauser et al., 2024; Brighenti et al., 2023).

3 Observed temporal and spatial data

3.1 Meteorological data

The daily meteorological station data are measured and used as inputs in the *WaSiM* hydrological model. 12 stations (Table 1 and Fig. 1a) are located in and around the Martell Valley with records of air temperature, precipitation, solar radiation, relative humidity, wind speed, and snow height from 1972 to 2024. The elevations of all stations vary from 1720 to 3328 m a.s.l. Hofmeister et al. (2023a) assessed the data quality and corrected the observation errors of these climate stations until 2020. We apply the same procedure to the extended time series between 2020 and 2024.

The spatial and temporal interpolation of the climate station data to the retained spatial grid (25 m × 25 m) is performed in the *WaSiM* modeling environment. *WaSiM* supports irregularly observed data (i.e., missing values) and uses the following interpolation methods: the solar radiation, relative humidity, and precipitation recorded at the observed stations are spatially interpolated at daily time steps with the Inverse Distance Weighting (IDW) method. The wind speed and air temperature are interpolated with a combined method of IDW and elevation-dependent regression. The potential evapotranspiration (PET) is calculated with the Penman-Monteith method (Brutsaert, 1982; Monteith, 1981) available in *WaSiM* by using the daily temperature, relative humidity, solar radiation, and wind speed.

The snow height (SH) data are measured at the Zufritt and Zufallhuette stations (Table 1). We transform the snow height to snow water equivalent (SWE) with the ΔSnow model (v1.0.2) available in the R package "*nixmass*" (Winkler et al., 2021). This model adopts a process-based multilayer method and considers the relationship between snow density (Pistocchi, 2016) and predefined regional parameters for Italy (Guyennon et al., 2019) in the SWE calculation. The SWE data are then used to calibrate the parameters of the snow module in *WaSiM* (Details on snow module calibration are given in Sect. 4.1).

3.2 Hydro(geo)logical data

We installed five groundwater piezometers in the river floodplains, which are relatively flat with the pre-assumed existence of groundwater storage (Fig. 1 and Table 2). The piezometers are located at elevations above 2300 m a.s.l. and in the same geological units (alluvial and fluvioglacial deposits, alpine postglacial synthemes, quaternary aquifer)

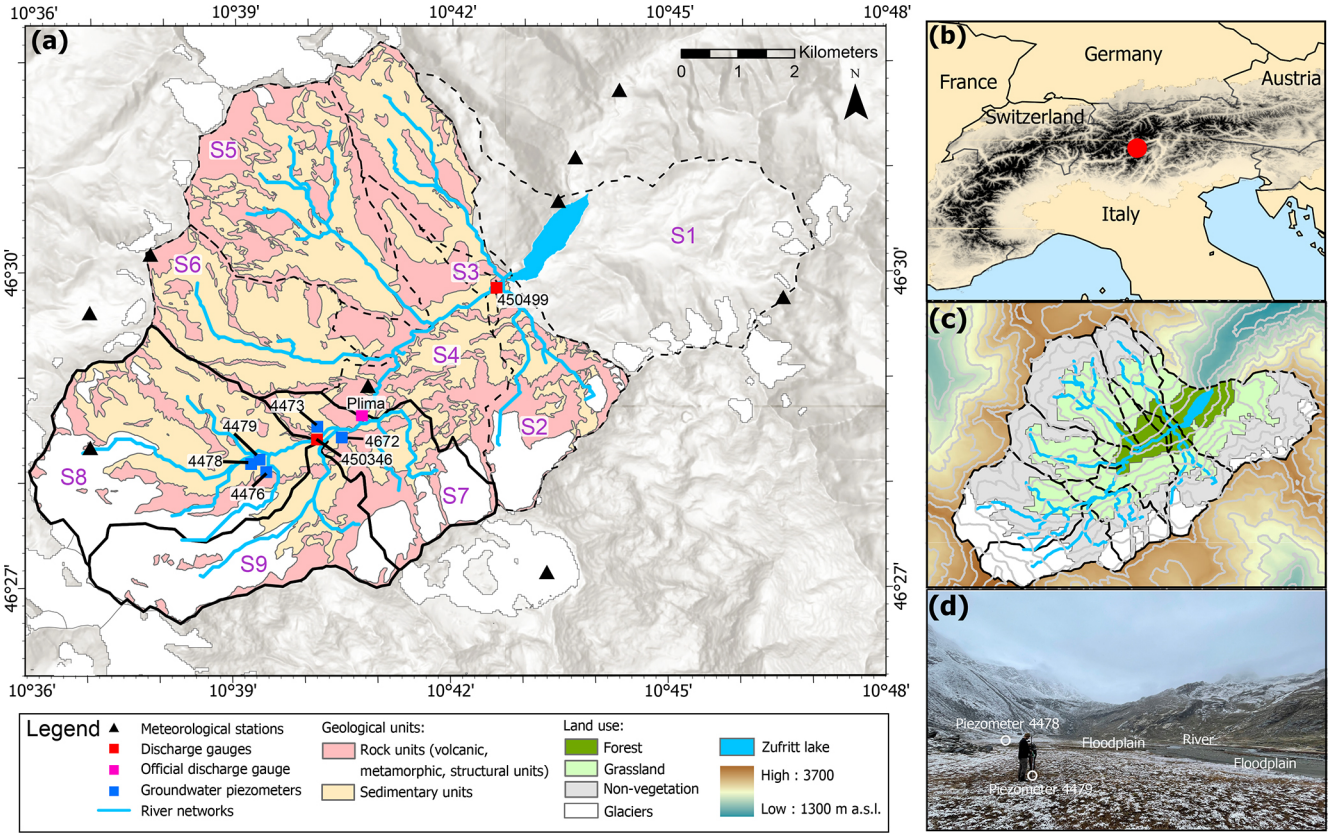

Figure 1. Maps of the Martell Valley in Northern Italy: **(a)** The zoomed-in map with the observed hydro-meteorological stations, with background characterized by geological units (Ramskogler et al., 2023; Berra et al., 2012). The numbers in black refer to the hydrological station IDs listed in Table 2 and the numbers (S1–S9) in violet refer to the subcatchment IDs. The white blocks denote the regional glacier coverage in 2000 (Knoflach et al., 2021). **(b)** The overview map shows the location of Martell Valley in the central European Alps. The dark shadow denotes the European Alps (Jarvis et al., 2008) and the red dot denotes the catchment location. **(c)** The land use map of the catchment (CORINE Land Cover, 2018): forest, grassland, glaciers (in 2006), rocks and soil (non-vegetation). The background is characterized by Digital Elevation Model data and contour lines (di Bolzano Alto Adige, 2006). **(d)** Fieldwork photo taken in November 2023 in the Subcatchment S8 (> 2400 m a.s.l.) where the piezometers ID 4478 and 4479 are located. © X.Fan. CORINE Land Cover © European Environment Agency (EEA). © Provincia Autonoma di Bolzano – Alto Adige. All rights reserved.

Table 1. Meteorological stations with daily records near the Martell Valley. Abbreviations: mean air temperature (T in [°C]), precipitation (P in [mm]), solar radiation (GS in W m^{-2}), relative humidity (LF in %), wind speed (WS in [m s^{-1}]), snow height (SH in [cm]).

Station name	Station ID	Longitude [°]	Latitude [°]	Elevation [m a.s.l.]	Start date	End date	Climate variables
Schoentaufspitze	06040WS	10.6286	46.5029	3328	2003.01.01	2024.01.15	T, WS
Madritsch	06090SF	10.6144	46.4938	2825	2003.01.01	2024.01.15	T, P, GS, LF, WS
Sulden	06400MS	10.5953	46.5159	1907	2003.01.01	2024.01.15	T, P, GS, LF
Hintermartell	11400MS	10.7269	46.5169	1720	2009.01.01	2024.01.15	T, P, GS, LF, WS
Weissbrunnspitz	24170WS	10.7740	46.4940	3253	2004.01.01	2024.01.15	T, P, GS, LF, WS
Rossbaenke	24300SF	10.8194	46.4693	2255	2002.01.01	2024.01.15	T, LF, WS
Weissbrunn	24400MS	10.8318	46.4868	1900	2002.01.01	2024.01.15	T, LF
Careser	T0065	10.6991	46.4226	2600	1990.10.01	2024.01.15	T, P, LF, WS
Ghiacciaio	T0473	10.7183	46.4513	3093	1990.12.01	2024.01.15	T, LF, WS
Langenferner	–	10.6139	46.4725	2967	2012.10.26	2023.10.02	T, GS, LF, WS
Zufritt	11200BM	10.7251	46.5090	1851	1972.01.01	2024.01.15	T, P, SH
Zufallhuette	16ZH	10.6781	46.4814	2265	2004.12.01	2023.02.23	SH

(Ramskogler et al., 2023; Berra et al., 2012). We also installed two river gauging stations which cover an elevation range of 1878 to 2347 m a.s.l. (Fig. 1 and Table 2). The river water levels are transformed to discharge with the rating curves of Hofmeister et al. (2023b). The main river (Plima) has its source at the Langenferner, flows through the catchment, and enters the Zufritt Lake in the northeast. The Plima official discharge station has been operated since 2014. All groundwater level and river discharge data are preprocessed in daily time steps for the hydrological model simulations.

Additionally, we collected groundwater and river water samples at the Piezometers ID 4478, 4479, and Stream gauge ID 450346 in the upper Subcatchment S8 in November 2022 and November 2023 to understand surface water-groundwater interactions at the onset of the low-flow season. The stable water isotopes (δ^2H and δ^{18}O) are analyzed in the laboratory in the Institute of Geography at the University of Bern with the cavity ringdown spectrometer "Picarro L2140-i" with autosampler and the attached vaporisation module "Picarro A0211". We follow the procedure described in the work of Meier (2024) (Sect. 3.2.1) to perform laboratory analysis of water samples and preprocessing of the isotope data.

We quantify the trends of the time-series hydrological variables with the non-parametric Mann-Kendall test (Kendall, 1962; Mann, 1945) and Sen's slope method (Sen, 1968). Statistical significance is assessed at the 5 % level (p-value $<$ 0.05) and uncertainty in the slope estimates is characterized using 95 % confidence intervals (CI). The MATLAB function *mannkendall* (v1.0.0) (Collaud Coen and Vogt, 2021; Collaud Coen et al., 2020) is adopted to first remove the first-order autocorrelation in the data with a 3PW pre-whitening procedure and then to quantify the trends.

3.3 Spatial data

The Digital Elevation Model (DEM) data of the study site are provided by the Province of Bolzano (di Bolzano Alto Adige, 2006) and available in a spatial resolution of 0.5 m × 0.5 m in 2006. The soil profile and attributes in 2018 are extracted from the Harmonized World Soil Database (HWSD, version 2.0) in a 1 km × 1 km resolution (FAO and IIASA, 2023; Ramskogler et al., 2023). The land use and land cover data of the site in 2018 are obtained from the Corine Land Cover Data Center (CORINE Land Cover, 2018) in a resolution of 100 m × 100 m (Fig. 1c). The geology map and geodatabase of the site are obtained from Ramskogler et al. (2023) and Berra et al. (2012). The glacier coverage maps of the site are obtained from Knoflach et al. (2021) and are available in the years 1850, 1911, 1959, 1985, 1997, 2005, 2013, 2017, and 2019.

All spatial raster data are resampled to the same spatial resolution with *ArcGIS Pro* (v3.1.0) for hydrological modeling. We adopt the modeling spatial resolution of 25 m × 25 m (after testing with 20, 50, 100 m) by balancing the trade-off between the computational intensity and the terrain complexity. As for many comparable high-elevation catchments, there is no detailed soil data available at this site. The available soil data may struggle to represent some small-scale features (e.g., moraine or similar glacier deposits) due to limited resolution (FAO and IIASA, 2023; Ramskogler et al., 2023).

We use the add-on software of *WaSiM* named *Tanalys* to generate the spatial grid data of local slope and flow accumulation based on the DEM data. These two variables are then used to calculate the Topographic Wetness Index (TWI) for each grid cell in the catchment to facilitate understanding the topographic control of the hydrological processes by using Eq. 1 (Pourali et al., 2016; Beven and Kirkby, 1979):

$$\mathrm{TWI} := \ln\left(\frac{a}{\tan\beta}\right), \tag{1}$$

where a [m^2] is the local upslope catchment area per unit contour length along the flow pathway; $\tan\beta$ is the local steepest downslope in radians by comparing the slope of the modeled grid cell with that of its neighboring cells.

4 Fully-integrated surface-subsurface hydrological modeling

We run the Water Balance Simulation Model (*WaSiM*) (Schulla, 2024, 1997) version 10.08.00 in daily time step and 25 m × 25 m spatial resolution. Different versions of the model have previously been used in many studies, such as for investigating fast local infiltration (Bronstert et al., 2023), snow process and redistribution (Förster et al., 2018; Warscher et al., 2013), impact of land use changes on streamflow (Cornelissen et al., 2013), and flash floods in the Mediterranean catchments (Garambois et al., 2013), but to our knowledge it has not been fully applied yet in high-elevation glaciated environments. *WaSiM* is a two-dimensional, fully-distributed, and modular-based hydrological model. It simulates hydrological partitioning and fluxes on a regular horizontal grid, with the stream network being represented as selected grid cells of the domain. The subsurface consists of a predefined number of soil layers, with groundwater situated at the bottom. Groundwater heads can fluctuate between these layers (Schulla, 2024). Lateral exchange is allowed between the soil grid cells that are adjacent to the stream network cells. The Darcy's law is implemented to simulate groundwater flow in the groundwater module (Schulla, 2024).

Besides the meteorological time series (air temperature, precipitation, solar radiation, wind speed, relative humidity), *WaSiM* also requires spatial gridded inputs, such as local slope, aspect, flow direction, flow accumulation, and river networks. These raster files are generated with *Tanalys* (Schulla, 2024) based on the DEM data. Each module in *WaSiM* can be flexibly activated depending on research needs. A detailed description of each module is available in

Table 2. Observed groundwater piezometers and river gauging stations in the Martell Valley. The Plima Station is an official station operated by the Autonomous Province of Bolzano in South Tyrol. The river gauge ID 450499 was destroyed during the extreme flooding events between 12 July and 9 August 2023.

Variable	Station ID	Longitude [°]	Latitude [°]	Elevation [m a.s.l.]	Start date	End date
Groundwater	4478	10.65186	46.46949	2454	2022/11/24	2023/11/01
Groundwater	4479	10.65302	46.47014	2455	2022/11/24	2023/11/01
Groundwater	4476	10.65507	46.46828	2447	2023/05/12	2023/11/01
Groundwater	4473	10.66646	46.47441	2333	2023/03/29	2023/11/01
Groundwater	4672	10.67205	46.47382	2319	2023/09/20	2023/11/01
River	450346	10.66730	46.47256	2347	2019/07/17	2023/11/01
River	450499	10.70838	46.49637	1878	2020/06/30	2023/08/07
River	Plima	10.67680	46.47630	2311	2014/06/01	2024/01/15

the works of Schulla (2024, 1997). Here, we focus on describing the key modules used to set up the fully-integrated surface-subsurface hydrological model in the Martell Valley, including the snow, glacier, unsaturated zone, and groundwater modules.

4.1 Snow and glacier modules

In *WaSiM* (Schulla, 2024), the snowfall is simulated with a threshold approach and a user-defined temperature-transition range. For snowmelt, we adopt the advanced energy-balance method together with the wind-driven and gravitational snow redistribution algorithms (Schulla, 2024; Thornton et al., 2021; Shrestha et al., 2014; Warscher et al., 2013; Gruber, 2007). This enables improved snow and river discharge simulations (Fig. S1 in the Supplement) compared with the commonly adopted temperature-index approach (Liu et al., 2025; Nan et al., 2025), but the associated shortcoming is the significantly increased computational demand and simulation time. The outflow from the snowpack infiltrates into the soil, which is solved with the Richards equation (Richards, 1931). The infiltration amount is the minimum between the fillable porosity of the uppermost soil layer and the total amount of rainfall and meltwater per time step. Surface runoff is generated by the infiltration excess and saturation excess of the soil moisture.

We adopt the dynamic glacier module (Schulla, 2024) to simulate the glacier area evolution by using a volume-area scaling approach (Bahr et al., 1997; Chen and Ohmura, 1990). In the glacier module, the glacier mass gain (due to snow accumulation) and melt (due to snow, firn, and ice melt) are calculated and balanced over each year in *WaSiM*. The transformation from snow to firn takes one year if the snow does not melt within one season, and from snow to ice takes seven years (Schulla, 2024). The model calculates the annual glacier mass balance, updates the glacier cover, and simulates snow metamorphism on 1 October of each year. The snow-on-ice melt is simulated with the same energy-balance approach as adopted in the Snow Module. As the energy-balance method is not available for simulating ice melt in *WaSiM*, we adopt the extended temperature-index approach (Hock, 1999, 1998) which allows us to include the solar radiation information at each daily time step when simulating the firn and ice melt (see Eq. 2.21.2 and 2.21.3 in the work of Schulla, 2024). The meltwater from snow-on-ice, firn, and ice is conceptually transformed into streamflow via a linear reservoir approach: each melt component is handled with a separate linear reservoir that has a specific storage coefficient (Schulla, 2024). We acknowledge the modeling uncertainty associated with the simplified assumption of the glacier drainage system during each melting period.

4.2 Unsaturated zone and groundwater model

All grid cells that are not stream grid cells contain a fixed number of unsaturated and saturated domain layers, which is set to five in total here (this applies also to glacier grid cells). Input to the unsaturated zone module is the sum of non-intercepted rainfall and meltwater from snow and ice (if present). Infiltration and vertical fluxes between the unsaturated soil layers are solved iteratively with the Richards equations (Schulla, 2024, 1997; Richards, 1931). The properties for each soil layer and for each soil type (i.e. soil in alpine grassland, podzol under coniferous forest, rocks) are defined per grid cell, such as soil depth, vertical hydraulic conductivity, and characteristics of the macropores (e.g., macropore capacity, reduction of macropore capacity per meter of soil depth) (Schulla, 2024). The macropore approach is implemented in *WaSiM* by following the "bypass-flow-concept" introduced in the work of Jansson and Karlberg (2004).

To simulate the groundwater head changes, the unsaturated zone is coupled with a horizontal two-dimensional groundwater model. Groundwater is situated at the bottom of the soil layers. For this reason, *WaSiM* requires the lower boundary of the aquifer to be identical to the lower boundary of the soil layers. The shallow aquifer is modelled as unconfined, given that the observed depth to water table (DTW) is mostly within 1 m. The groundwater formulation is therefore primarily intended to represent the shallow unconfined aquifer system constrained by the available piezometer ob-

servations, while deep groundwater flow is beyond the scope of the present model configuration. The unsaturated zone module first computes the vertical flux (i.e., the percolation) from the lowest unsaturated soil layer to the groundwater. This flux is then taken as the upper boundary condition for the groundwater model to calculate the lateral fluxes, which are solved with the Darcy equation. The net changes of the groundwater table are converted into a vertical flux, which is given back to the lowest unsaturated soil layer as inflow or outflow (Schulla, 2024). Five parameters in the groundwater model are calibrated with the observed groundwater heads measured at the piezometers (Table 4), including the horizontal hydraulic conductivities, storage coefficient, lower boundary of the aquifer, and colmation of the soil, which is a term used in *WaSiM*: it controls the water exchange rate between the adjacent saturated soil cells and the river cells. The groundwater heads are assumed to be constant beneath the glacierized cells, which is a built-in feature in the model (Schulla, 2024).

4.3 Streamflow generation

The generation of streamflow based on water mobilized at the level of grid cells follows two stages: First, the surface runoff and the subsurface lateral flow ("interflow") in the unsaturated zone are computed per grid cell; they are then transformed separately to the stream by a single reservoir cascade (isochrone approach with additional retention in each class, see details in Schulla, 2024). *WaSiM* applies a flow travel time concept at each time step in the reservoir cascade to ensure temporal synchronization of each flow component (Eq. 2.12.13 in the work of Schulla, 2024). The surface runoff is generated when saturation excess of soil moisture or Hortonian infiltration excess occurs. The subsurface lateral flow for each layer per grid cell is generated based on the water content of the soil layer, hydraulic conductivity, and local slope. Baseflow contribution to streamflow is obtained via direct lateral exchange of adjacent saturated soil cells to river cells. The stream grid cells are generated from the DEM using the *Tanalys* add-on of *WaSiM* and are aligned with the observed stream locations as closely as possible. The stream network topology itself is static in the model. The average values of each streamflow component (surface runoff, subsurface lateral flow, and baseflow) are summed up to the total streamflow, which is the input to the routing model (Schulla, 2024).

4.4 Model calibration and evaluation

4.4.1 Calibration parameters

Here we summarize the parameters to be calibrated in each *WaSiM* module. In the snow module, 11 key parameters which govern snow accumulation, snow ablation, wind-driven and gravitational snow redistribution are calibrated (Table 3). Specifically, the calibrated parameters "TRS" and "Ttrans" (0 and 2 °C) define a linear transition of snow fraction from 100 % at −2 °C ("Ttrans"), 50 % at 0 °C ("TRS"), to 0 % at +2 °C ("Ttrans"). In the glacier module, 7 key parameters which govern the initialization of glacier volume and the ice and firn melt are calibrated (Table 3). The average equilibrium line elevation (ELA, m a.s.l.) in the model is set to 2900 m a.s.l. based on the observations at the Langenferner glacier in 2006 (Autonome Province of Bolzano, 2007). The volume-area scaling factor is set to 28.5, adopted from the work of Chen and Ohmura (1990), and the exponent is set to 1.375 according to the work of Bahr et al. (2015).

The parameters in the subsurface module are calibrated using the observed groundwater heads at the piezometers in the upper headwater subcatchments (S7–S9, Fig. 1). The lower boundary of the soil layers is calibrated to be 1.30 m (see details in Sect. S3 and Figs. S4–S8 in the Supplement); the properties for each soil layer (vertical heterogeneity) and each soil type (i.e. soil in alpine grassland, podzol under coniferous forest, rocks, for representing horizontal heterogeneity) are defined per grid cell, such as hydraulic conductivity and characteristics of the macropores. In the groundwater model, the aquifer hydraulic conductivity, storage coefficient, and colmation of the soil are calibrated. A total of 13 parameters are calibrated and their values are provided in Table 4. Many calibrated groundwater parameters are found to be identical at the 5 piezometers, likely due to similar local geology and water fluctuation depths (Fig. 1 and Sect. 2). Initial sensitivity analyses indicate that the remaining parameters are rather insensitive; the default values suggested for each soil type from the user manual (Schulla, 2024) are hence adopted for them. This study focuses on the upper subcatchments (S7–S9), where the majority of hydrological stations and groundwater piezometers are installed and where the simulated results have high confidence. Nevertheless, we also modeled the whole catchment by transferring the subsurface parameters from the upper subcatchments to the ungauged area with the aim of providing a catchment-scale overview, while acknowledging that the overview results may contain higher uncertainty, especially in the valley floor due to a lack of deep groundwater observations.

4.4.2 Calibration and evaluation procedure

Each model simulation with a selected parameter set runs from 1 October 2006 to 15 January 2024 in a 25 m × 25 m gridded resolution at daily time steps. Because of long temporal and high spatial resolution adopted for the fully-distributed physics-based modeling, a complete simulation takes around 10 h to run on a computer with 6 computational cores (Processor: 13th Gen Intel(R) Core(TM) i7-1370P 1.90 GHz). The first 5 years (1 October 2006–30 September 2011) are considered as the spin-up period, as the glacier and subsurface water storage modules take time to stabilize to produce reasonable simulations (Hofmeis-

Table 3. Calibrated parameters in the snow and glacier modules in *WaSiM* (Schulla, 2024, 1997). Parameters with no unit are denoted with [–].

Module	Parameter	Description	Value
Snow accumulation	TRS	Temperaure at which half of the precipitation falls as snow [°C]	0
Snow accumulation	Ttrans	Half of the temperature range from snow to rain [°C]	2
Snow ablation	LWINcorr	Correction factor for incoming long-wave radiation [–]	1.2
Snow ablation	LWOUTcorr	Correction factor for outgoing long-wave radiation [–]	1.0
Snow gravitational redistribution	i_lim	Max. deposition slope [°]	55
Snow gravitational redistribution	D_lim	Scaling for max.deposition [mm]	2
Snow gravitational redistribution	i_erosion	Min. slope for creating slides [°]	50
Snow gravitational redistribution	f_erosion	Fraction of snow pack forming the slide [–]	0.007
Wind-driven redistribution	Start azimuth	First quantile of wind direction [°]	179
Wind-driven redistribution	End azimuth	Third quantile of wind direction [°]	217
Wind-driven redistribution	cmin	Min. correction factor [–]	0.5
Glacier initialisation	VA_scale	Volume-area scaling factor [–]	28.5
Glacier initialisation	VA_exp	Volume-area exponential factor [–]	1.375
Glacier initialisation	WEchnge	Change rate of water equivalent per m [mm]	1.8
Glacier initialisation	ELA	Average equilibrium line elevation [m a.s.l.]	2900
Glacier melt	MF	Melt factor [mm]	2
Glacier melt	ice_min	Min. radiation coefficient for ice [mm $Wh^{-1}\,m^2\,°C^{-1}\,d^{-1}$]	0.0001
Glacier melt	ice_max	Max. radiation coefficient for ice [mm $Wh^{-1}\,m^2\,°C^{-1}\,d^{-1}$]	0.0007

ter et al., 2022). The rest (1 October 2011–15 January 2024) is used for model calibration and evaluation. Given the large number of parameters, the complicated surface-subsurface hydrological processes (snow-glacier-vegetation-river-unsaturated zone-groundwater), and the complex topography where the elevation ranges around 2000 m (1777 to 3743 m a.s.l.), the computationally intensive automatic calibration is not adopted. Instead, we tackle this task by adopting a multi-signal calibration approach to calibrate the model from top to bottom and module by module with the relevant reference data. The sequential calibration of module by module is a commonly adopted logical procedure to calibrate fully-distributed physics-based hydrological models (Fatichi et al., 2015). We first analyze the sensitivity of the key parameters in each module. We then perturb and calibrate the identified sensitive parameters in detail to the observed variables.

Specifically, to calibrate the groundwater module using point-scale groundwater level observations, we extract an ensemble of simulated groundwater level time series from the predefined model grid cells located in the vicinity of each observation borehole within the model domain. The resulting ensemble of grid-cell simulations is then compared against the observed groundwater level records at the corresponding borehole locations. Subsurface model parameters were subsequently adjusted based on the discrepancies between simulated and observed groundwater levels to improve model performance.

Table 4. Calibrated parameters in the unsaturated zone and groundwater model in *WaSiM* (Schulla, 2024, 1997). Parameters with no unit are denoted with [–]. The hydraulic conductivity (ksat) is calibrated for each land cover category, and the range indicates the variations of hydraulic conductivity between the soil layers vertically. Other parameters are assumed to remain constant, given that all boreholes are situated in the same hydrogeology category. The colmation of the soil is a term used in *WaSiM* that controls the water exchange rate between the adjacent saturated soil cells and the river cells.

Module	Parameter	Description	Value
Unsaturated zone	kd	Storage coefficient of direct flow [–]	2
Unsaturated zone	ki	Storage coefficient of subsurface lateral flow [–]	10
Unsaturated zone	dr	Scaling factor applied to river drainage density [–]	0
Soil table	krec	Recession constant for the saturated conductivity with depth [–]	1
Soil table	PMThr	Macropore threshold [$mm\,h^{-1}$]	2
Soil table	MRedu	Capacity reduction [m^{-1}]	1
Soil table	Depth	Lower boundary [m]	1.30
Soil table	ksat	Vertical hydraulic conductivity [$m\,s^{-1}$]	$4\times10^{-4}\sim6\times10^{-6}$ (forest area) $2\times10^{-4}\sim5\times10^{-7}$ (alpine grassland) $1\times10^{-5}\sim8\times10^{-7}$ (rocks)
Groundwater	Input grid (.aq1)	Lower boundary [m]	1.30
Groundwater	Input grid (.kol)	Colmation of the soil [$m\,s^{-1}$]	1×10^{-6}
Groundwater	Input grid (.kx,.ky)	Horizontal conductivity [$m\,s^{-1}$]	5×10^{-5}
Groundwater	Input grid (.s03)	Storage coefficient [–]	0.3

The module-by-module calibration provides good diagnostic power, as it isolates which modules (e.g., snow, glacier) are causing discrepancies between observation and simulation. This enables an incremental validation, as each module can be tested and validated before being integrated with the next. By doing so, errors in specific processes (e.g., snow or glacier melt) can be addressed without compromising other well-performing modules. Despite the calibration being sequential, we rerun the whole model (including all modules) each time when the parameters in a module are perturbed, and we focus on the model performance of that module. In this way, the hydrological processes between the modules are interconnected and the consistency is ensured. It is worth mentioning that building up a physics-based, fully-distributed hydrological model requires numerous details about the catchment to constrain the model parameters, and it is practically challenging. The purpose of our model is, however, not to reproduce exactly the catchment, but to understand the hydrological processes and to test hypotheses by using a reasonable parameter set, and that the simulated dynamics (relative changes) in the system should be reasonably consistent (Engdahl, 2024).

4.4.3 Reference signals and performance criteria

In the multi-signal calibration, the simulated spatial SWE in *WaSiM* is calibrated to (i) the fractional snow-covered area derived from the MODIS daily snow cover maps (2002–2019) (Matiu et al., 2019) performed by Hofmeister et al. (2022) and (ii) the observed SWE at the in-situ stations from 2006 to 2024 (see Sect. 3.1). The glacier module is calibrated to (i) the observed fractional glacier-covered area (which is calculated as the glacier area divided by the catchment area), and (ii) the annual glacier mass balance of the Langenferner glacier (2006–2021) in the Subcatchment S8 (Galos et al., 2017; Autonome Province of Bolzano, 2007). The subsurface modules are calibrated to the observed groundwater hydrographs at the piezometers. The three gauging stations

listed in Table 2 are adopted to evaluate the simulated discharge.

We select satisfying model parameters via visual comparison between the simulation and observation for different reference datasets (SWE, discharge, and groundwater heads). We also evaluate the goodness-of-fit of the model with the Nash-Sutcliffe Efficiency (NSE) (Nash and Sutcliffe, 1970), Mean Absolute Error (MAE), and Root Mean Square Error (RMSE). Due to uncertainties in the measured discharge and groundwater heads, the Spearman's rank correlation coefficient (ρ) is also adopted to evaluate the model performance (Gauthier, 2001). Statistical significance is assessed at the 5 % level (p-value < 0.05).

5 Results

5.1 Snow and glacier observations and simulations

Figure 2 shows the observed and simulated snow and glacier changes and melt rates in the Martell Valley. The simulated snow water equivalent (SWE) time series extracted from the gridded results capture well the observed snow dynamics at different elevations (Zufritt Station: NSE of 0.87, Spearman's rank correlation coefficient of 0.93 with a p-value < 0.001, MAE of 25.09 mm w.e., RMSE of 50.30 mm w.e.. Zufallhuette Station: NSE of 0.74, Spearman's rank correlation coefficient of 0.88 with a p-value < 0.001, MAE of 47.52 mm w.e., RMSE of 60.46 mm w.e.). The simulation also reproduces well the interannual variability of snow accumulation and the severe snow droughts in the recent past, for example, with the simulated peak snow accumulation in 2012, 2017, 2022, and 2023 being as low as 138, 103, 112, and 111 mm w.e., which are well below the mean of 316 mm w.e. computed over the evaluation period of 2011–2023 at the Zufritt Station (see Fig. 2a, b). The snow drought in 2022 was observed not only in the Martell Valley but also in the Po Basin in Italy (Avanzi et al., 2024). Hofmeister et al. (2022) adopt the same snow parameter set and show comparable performance between the simulated snow cover and the remote sensing data from Sentinel-2. The simulated snow dynamics and distribution are further used to simulate the hydrological changes in this study.

Like in most glaciated catchments, the observed fractional glacier coverages (glacier area divided by the whole catchment area) are very sparse, but they remain helpful to understand the glacier module performance (Fig. 2c). The observed fractional glacier coverage shows a declining trend since 1850, except for the period around 1985 showing an increase. The glacier module first takes time to stabilize during the spin-up period (2006–2011). In the evaluation time frame after the spin-up years, the model shows decreasing rates of fractional glacier coverage close to the observation with a slight overestimation of ~ 1 %. This slightly overestimated glacier coverage is primarily because of a few non-existent small glaciers appearing due to preferential snow deposition along northeast exposed mountain ridges in the model. The simulated catchment cumulative glacier mass balance (zoomed-in plot in Fig. 2c) shows a strong seasonality and a significant decreasing trend of -1.21 m w.e. $^{-1}$ (p-value $<$ 0.001, 95 % CI: -1.39 to -1.10 m w.e. yr^{-1} during the evaluation period 2011–2023), which is close to the average glacier mass changing rate (-1.29 ± 0.28 m w.e. yr^{-1} from 2015 to 2024) in central Europe (Dussaillant et al., 2025). Additionally, the glacier module is calibrated to the annual glacier mass balance of Langenferner glacier located in the Subcatchment S8 (Fig. 1d). Apart from the spin-up period, the model captures well the general dynamics of the Langenferner glacier mass evolution in both mass-growing years (in 2014) and in loss years. The model simulates well the mean annual glacier mass balance of Langenferner glacier (both simulation and observation are equal to -1.02 m w.e. in the evaluation period between 1 October 2011 and 30 September 2021, Fig. 2d). Nevertheless, it struggles to capture the observations in a few years (i.e., in 2013, 2016, and 2018). This could be because only the Langenferner's glacier mass balance data are available for estimating the parameters of the glacier module. However, glacier mass balance is not only affected by meteorological forcings, but also other environmental factors, such as aspect and elevation (Zhang et al., 2022). Other glaciers in the catchment may hence respond in a slightly different way due to these non-climatic factors (Nan et al., 2025; Müller et al., 2024). Another reason could be that the volume-area scaling factor approach struggles to account for ice flow and tends to underestimate glacier volumetric changes, especially in the accumulation phase (Schaffhauser et al., 2024).

The total annual liquid water input into the catchment (called "precipitation equivalent" or PEQ hereafter) is composed of annual rainfall, snowmelt, and glacier melt. *WaSiM* calculates and outputs the following melt components: snowmelt on the non-glacierized cells, snowmelt on the glacierized cells, firn melt on the glacierized cells, and ice melt on the glacierized cells. The snowmelt reported here is the summed snowmelt occurring both on the glacierized and non-glacierized cells; the reported glacier melt is the summed firn melt and ice melt. Figure 2e shows the annual magnitude of each flux (rainfall, snowmelt, glacier melt) between 2006 and 2023. We quantify the trend of each component starting from 1 October 2011 after the spin-up period. The annual rainfall, snowmelt, and glacier melt amount to 35 %, 45 %, and 20 % of the simulated annual PEQ on average (2011–2023). The PEQ shows a decreasing trend of -21 mm w.e. yr^{-1} (p-value $= 0.13$, 95 % CI: -51 to $+10$ mm w.e. yr^{-1}). The estimated annual trends of the flux components are -5 mm yr^{-1} for rainfall (p-value $= 0.50$; 95 % CI: -19 to $+4$ mm yr^{-1}), -26 mm yr^{-1} for snowmelt (p-value $= 0.10$; 95 % CI: -62 to $+4$ mm yr^{-1}), and $+10$ mm yr^{-1} for glacier melt (p-value $= 0.16$; 95 % CI: -5 to $+30$ mm yr^{-1}). These results indicate that

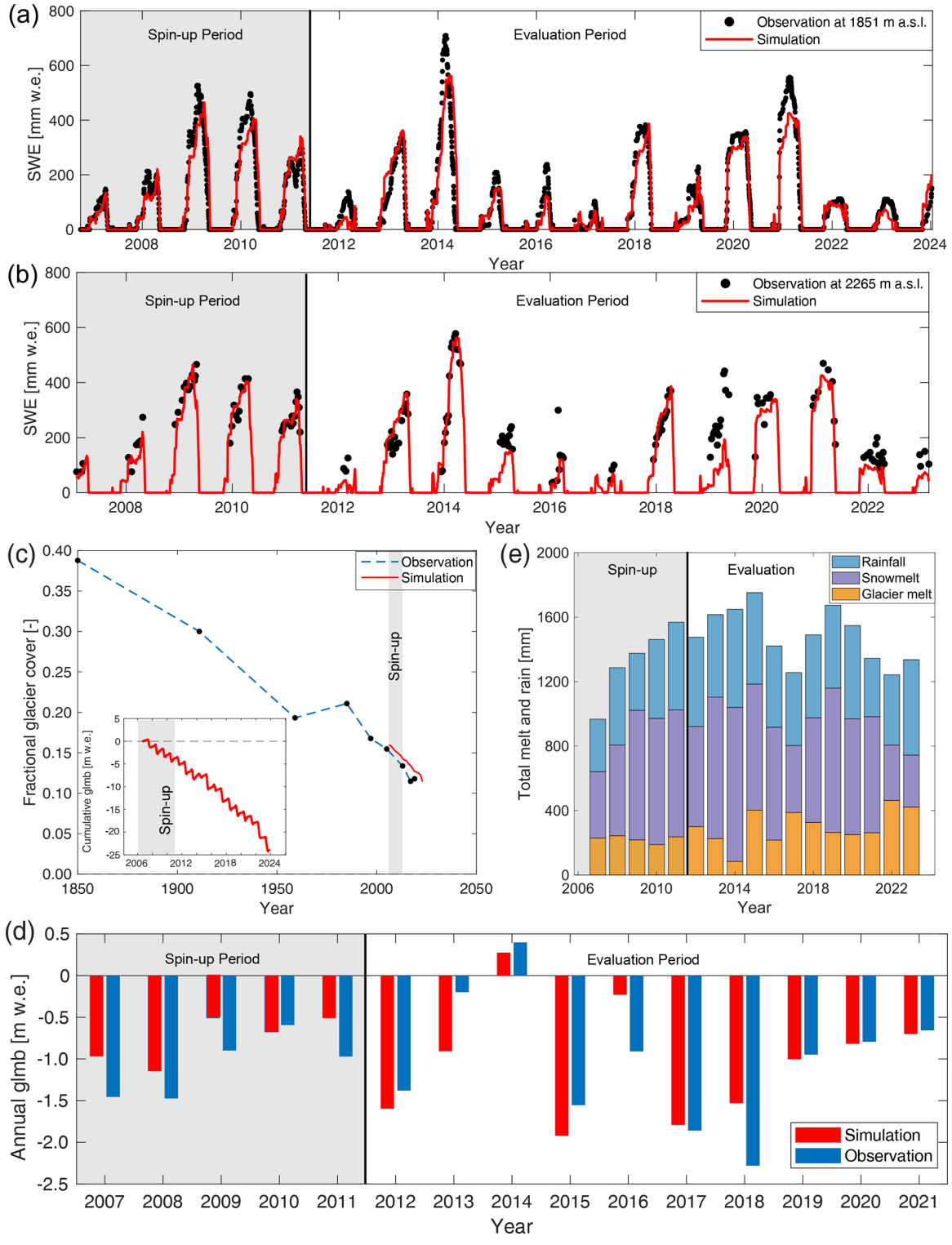

Figure 2. Observed and simulated snow and glacier changes in the Martell Valley. **(a–b)** The observed and simulated daily snow water equivalent (SWE) in mm w.e. at the **(a)** Zufritt and **(b)** Zufallhuette Stations (elevations: 1851 and 2265 m a.s.l. in Table 2). **(c)** The annual catchment fractional glacier coverage (i.e., glacier area divided by the whole catchment area) observed between 1850 and 2019 and simulated between 2006 and 2023. The zoomed-in plot shows the simulated catchment cumulative glacier mass balance (glmb) between 2006 and 2023. **(d)** The observed annual glacier mass balance of Langenferner glacier compared with the simulation of Subcatchment S8. **(e)** The simulated catchment annual total liquid flux (snowmelt, glacier melt, and rainfall) between 2006 and 2023. Spin-up period (5 years): 1 October 2006–30 September 2011, evaluation period: starting from 1 October 2011.

none of the flux components exhibit statistically significant trends over the study period. Among them, snowmelt shows the strongest decreasing tendency, whereas rainfall and glacier melt display comparatively weaker trends. However, the confidence intervals of all three components span both negative and positive values, indicating high uncertainty in the magnitude and direction of the long-term changes.

5.2 Hydro(geo)logical response to peak melts and rainfall events

Figure 3a characterizes the response of the observed river water level and shallow groundwater heads to the simulated hydrological inputs from rainfall, snowmelt, and glacier melt between November 2022 and November 2023 in the upper headwater Subcatchment S8 (subcatchment area: 12.3 km^2 with 31 % of glacier coverage, Fig. 1a). The observed river and groundwater records are used here as independent response variables, while the simulated fluxes characterize the timing and magnitude of the water inputs to the subcatchment. This comparison provides an observational basis for examining the relative timing of river and shallow groundwater responses to melt and rainfall events. The corresponding groundwater and streamflow simulations are evaluated separately against observations in Sect. 5.3 and 5.4. The groundwater boreholes (IDs 4479 and 4478) have a similar elevation (2455 m and 2454 m a.s.l.) and are both located around 30 m away from the river on the same side (Fig. 1 and Table 2). During the winter between November 2022 and April 2023, the river shows a slow recession and a low water level, corresponding to $< 0.5\ m^3\ s^{-1}$ of streamflow discharge or to $< 3.5\ mm\ d^{-1}$. This low winter streamflow is classically observed in many high-elevation catchments (> 2200 m a.s.l.) (Schmid, 2024) and can result from groundwater baseflow, leaked glacier melt, and ground heat-induced snowmelt (Müller et al., 2024). The groundwater heads at borehole ID 4479 exhibit relatively stable and slow dynamics during the cold months. In contrast, the neighboring borehole ID 4478, which is 115 m away from borehole ID 4479, shows a strong recession and drop-down of the heads. These results underline the heterogeneous groundwater dynamics in high-elevation Alpine catchments.

In May 2023, the river water level and both groundwater heads (IDs 4479 and 4478) were responsive to the early snowmelt and rainfall. Again, the groundwater borehole ID 4478 shows a much higher water level fluctuation (0.88 m) compared to the river gauge (0.24 m) and the other borehole ID 4479 (0.26 m). However, starting from glacier melt onset in June and in particular after glacier melt intensification in July (Fig. 3b), the two boreholes show similar dynamics and responses to the total PEQ, in contrast to their different behaviors in winter and early summer. During the warm period, the river water level and the groundwater heads are all responsive to the snow and glacier melts and extreme rainfall events, such as those in August and September. Unlike the deep-circulated groundwater, which may show a long lag time in response to surface conditions, the shallow groundwater heads observed in this study increase as quickly as the river water level during the peak melts (e.g. May 2023) and extreme rainfall events in the headwater landscape. Overall, these results imply the needs of a precise partitioning of the liquid fluxes (rainfall, snow and glacier melt) between the surface and subsurface for improving hydrological simulations.

5.3 Groundwater observation and simulation

Figure 4 shows the observed and simulated groundwater heads at five groundwater boreholes (in the upper Subcatchments S7 and S8 in Fig. 1 and Table 2) under model configurations with and without the *WaSiM* interflow component which represents lateral flow within the unsaturated zone. All observed boreholes measure the heads of unconfined shallow aquifers within the depth to water table (DTW) of 1.2 m. Our extensive parametric analyses show that the best simulations at all boreholes are achieved when the *WaSiM* interflow is constrained to zero (Sect. S4 and Figs. S9–S13 in the Supplement). The Spearman's rank correlation coefficients (p-value < 0.001) of the best simulations against the observations are 0.89, 0.84, 0.41, 0.61, and 0.81 for borehole IDs 4479, 4478, 4476, 4473, and 4672 (Fig. 4a–e). The MAE are 0.09, 0.31, 0.15, 0.18, 0.05 m and the RMSE are 0.14, 0.41, 0.20, 0.21, 0.07 m. The NSE ranges between 0 and 0.4 though. By visual comparison, the simulations captured well the observed temporal dynamics, such as the head response to the early and peak snowmelt and to the extreme rainfall events. The magnitudes of water table fluctuations are also well modeled at most of the sites, except for borehole ID 4478 (Fig. 4b) where the strong recession behavior in winter is challenging to simulate. When the *WaSiM* interflow is allowed, the simulated groundwater hydrographs (blue and purple lines in Fig. 4) underestimate the observed groundwater heads (black lines) and struggle to reproduce the observed temporal dynamics. That is, within the adopted model structure and parameterization, the daily shallow groundwater observations can be reproduced without requiring the *WaSiM* interflow component. This result highlights a model-diagnostic constraint on the representation of unsaturated-zone flow pathways in a fully-distributed high Alpine model. Independent field-based evidence is further needed to evaluate the physical relevance of this result and to test the associated hypothesis that subsurface lateral flow may play a limited role in runoff generation in such headwater environments. Given that the piezometers are located predominantly in a relatively flat floodplain (alluvial) setting, the observations do not directly constrain lateral flow processes along steep hillslopes. Further evidence might be obtained from hillslope piezometer transects, although these are highly challenging to install in high Alpine terrain, or from distributed soil moisture observations, for example us-

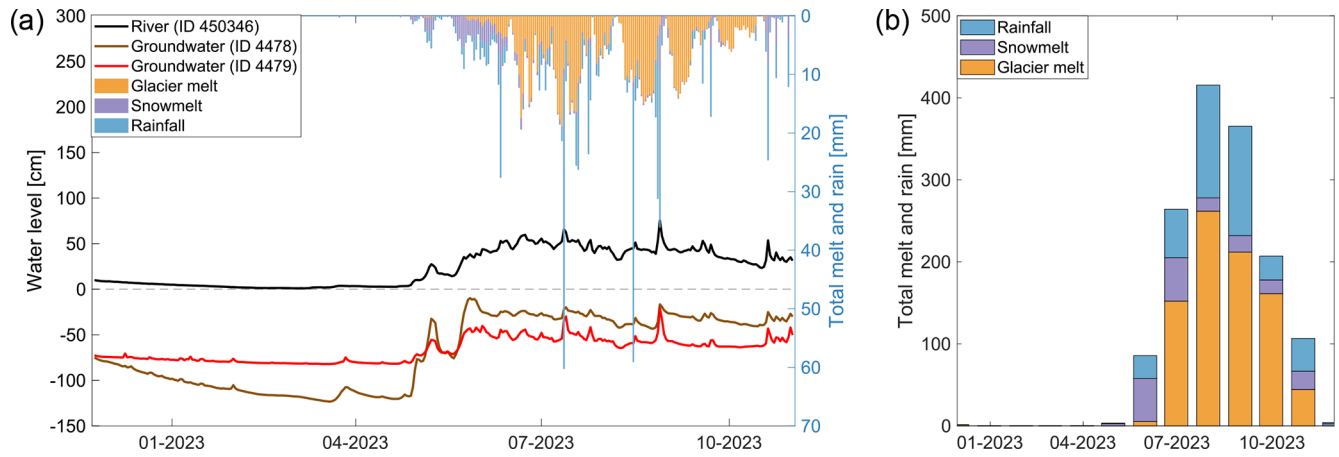

Figure 3. Hydrological response of the river and groundwater level to the total rainfall, snow, and glacier melts between November 2022 and November 2023 in the glaciated headwater Subcatchment S8 (Fig. 1) in the Martell Valley. **(a)** The observed daily river and groundwater level hydrographs and the simulated total daily meltwater and rainfall with *WaSiM* in this subcatchment. The reference level for river water level is the riverbed, with zero indicating dry conditions. The reference level for groundwater is the ground surface. The station elevations are provided in Table 2. The black line denotes the river water level measured at the gauge Upper Plima (ID 450346) in cm d^{-1}. The red and brown lines denote the groundwater heads measured at the boreholes ID 4479 and ID 4478 in cm d^{-1}. The stacked bars on the top denote the simulated daily glacier melt, snowmelt, and rainfall in mm d^{-1}. **(b)** The simulated monthly total snowmelt, glacier melt, and rainfall in this subcatchment in mm per month. The yellow blocks denote the glacier melt, the purple blocks denote the snowmelt, and the blue blocks denote the rainfall.

ing Electrical Resistivity Tomography (ERT) (Müller et al., 2022) or surface proxies such as repeated drone imagery to map the temporal occurrence of local saturation (Glaser et al., 2018).

To characterize the local topographic model setting associated with the groundwater recession discrepancy at some locations in the model domain (e.g., bore ID 4478), we compute the Topographic Wetness Index (TWI, Eq. 1) from the DEM (Pourali et al., 2016; Beven and Kirkby, 1979). Here, TWI represents topographic controls as resolved by the model. It is therefore influenced by the DEM quality and spatial discretization, which may slightly differ from the exact topographic conditions in the field (Pourali et al., 2016; Beven and Kirkby, 1979). The TWI ranges from 2.7 to 23.4 across the catchment, with a mean of 6.0, and higher values generally indicate a stronger tendency toward wet conditions in the model. We further quantify the relationship between TWI and simulated annual mean groundwater heads at the five boreholes and their surrounding grid cells. The relationship between these two variables shows to be positive at all locations (Fig. S3 in the Supplement).

Figure 5a–b show the spatial distribution of TWI in the upper headwater Subcatchments S7–S9 (Fig. 1), where the groundwater boreholes are installed. Boreholes ID 4479 and 4478 have similar local geology, land use, and soil properties, but differ markedly in their modeled topographic setting. Borehole ID 4479 has a TWI of 7.1 and its simulation captures the observed groundwater head variations reasonably well, whereas borehole ID 4478 has a higher TWI of 10.7, indicating a stronger modeled topographic tendency toward wet conditions. Considered alongside the relationship between TWI and groundwater level identified above (Fig. S3 in the Supplement), the result indicates that TWI (the modeled topographic control) can be useful as a diagnostic of spatial groundwater behavior in the model. The remaining discrepancy at borehole ID 4478, however, might also reflect the unresolved fine-scale topography, subsurface heterogeneity, or the spatial discretization (Riihimäki et al., 2021; Rinderer et al., 2014; Grabs et al., 2009).

To further quantify the simulation uncertainty, we summarize the ensemble simulations of neighboring cells using their median and interquartile range (Fig. S14). Nevertheless, the individual neighbouring-cell hydrographs are retained as diagnostic information, given that the strong local topographic heterogeneity in high Alpine catchment can produce markedly different groundwater responses over short distances (Fig. 5c–d). Defining the spatial support of a point-scale piezometer observation a priori is hence challenging, and simple spatial averaging may smooth local groundwater dynamics. The best-matching neighbouring cell is used primarily as a diagnostic indication that the model can reproduce the observed local dynamics, whereas the neighbourhood statistics provide the primary measure of spatial representativeness uncertainty. Resolving the exact point-scale response would require finer spatial discretization and a more detailed representation of local subsurface heterogeneity.

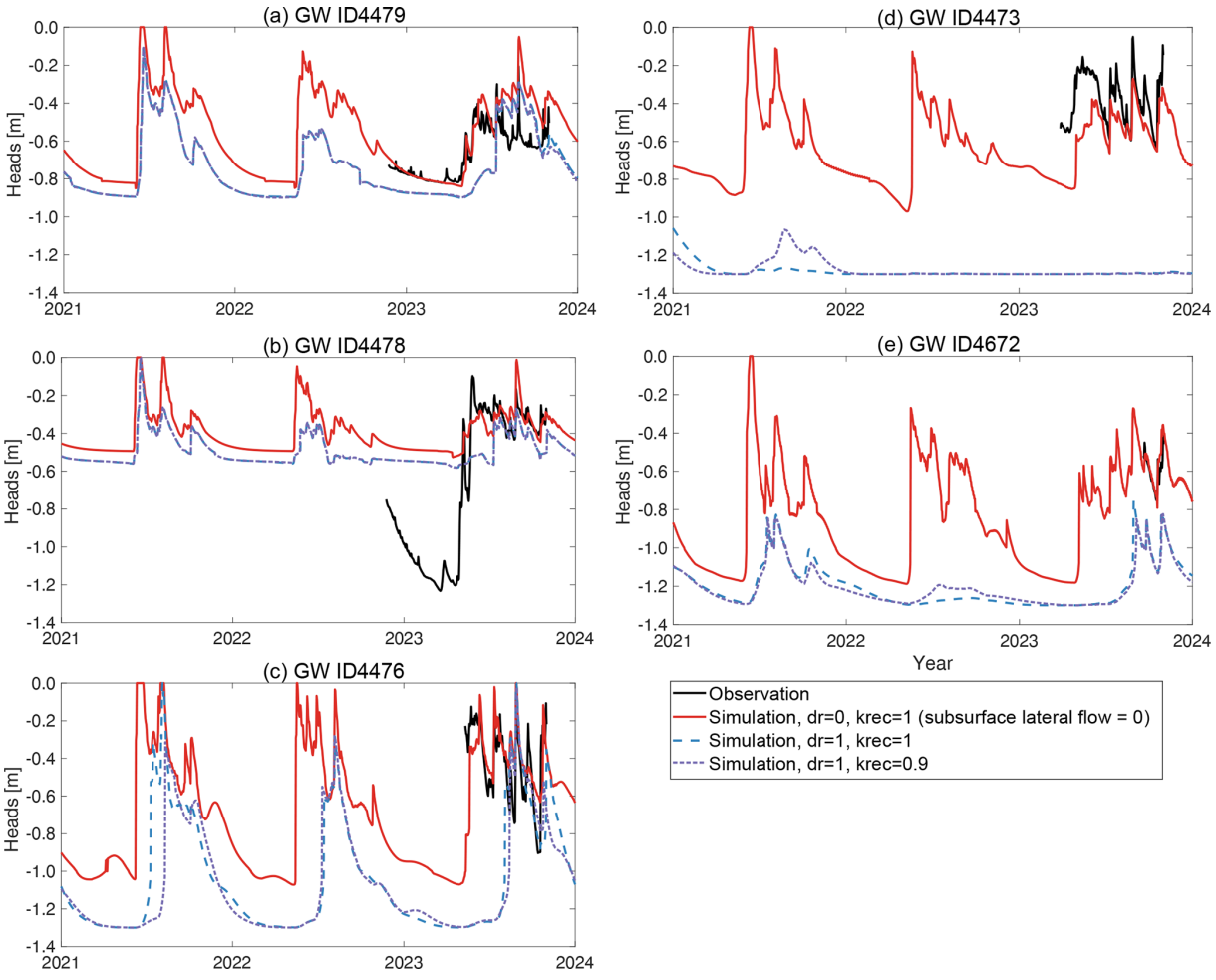

Figure 4. Observed and simulated groundwater heads at five piezometers in the upper headwater Subcatchments S7 and S8 (Fig. 1) with and without the *WaSiM* interflow component in the model. The groundwater heads are recorded as depth to water table (DWT) below the land surface. The black lines denote the observed hydrographs; the red lines denote the simulations without the *WaSiM* interflow component (subsurface lateral flow) by setting the parameters of dr = 0 and krec = 1; the blue and purple dashed lines denote the simulations with the *WaSiM* interflow allowed by slightly perturbing the dr and krec parameters.

5.4 River observation and simulation

Figure 6 shows the observed and simulated river discharge at three gauging stations (Fig. 1). At the gauging station ID 450346 which is located in the upper headwater Subcatchment S8, the simulated and observed discharges have a Spearman's rank correlation coefficient of 0.90 (p-value < 0.001), an NSE of 0.76, an MAE of 0.24 $m^3\,s^{-1}$, and an RMSE of 0.40 $m^3\,s^{-1}$ (Figs. 6a and S2c in the Supplement). The model captures well the temporal dynamics of the observed discharge in terms of response timing to the early and peak snowmelt and extreme rainfall events, despite the slight underestimation of the very low winter discharge and occasional overestimation of the peak discharge in the extreme rainfall events.

At the official discharge station Plima located in the Subcatchment S7, the model captures well the observed temporal discharge dynamics (Spearman's rank correlation coefficient: 0.90 with a p-value < 0.001, NSE: 0.63, MAE: 1.05 $m^3\,s^{-1}$, RMSE: 1.49 $m^3\,s^{-1}$, see Figs. 6b and S2b in the Supplement). Nevertheless, the model struggles to fully capture the winter low-flow dynamics in some years. The observed winter low flow has an annual mean of 0.59 $m^3\,s^{-1}$ or 2.0 mm d^{-1} (between December and March from 2018 to 2024) given the subcatchments area of 25.3 km^2, which is not uncommon for corresponding elevations (> 2400 m a.s.l.). But there appears to be more measurable winter low flow in 2019 and 2020 which are not captured by the model. The measured quick drop in winter discharge in 2021 was more likely due to instrument errors under frozen conditions (e.g., the sensor is frozen during low temperatures). Similar to station ID 450346, the model occasionally overestimates the high flow rates. This could partly be attributed to the uncertainty in the observed discharge, which is computed from

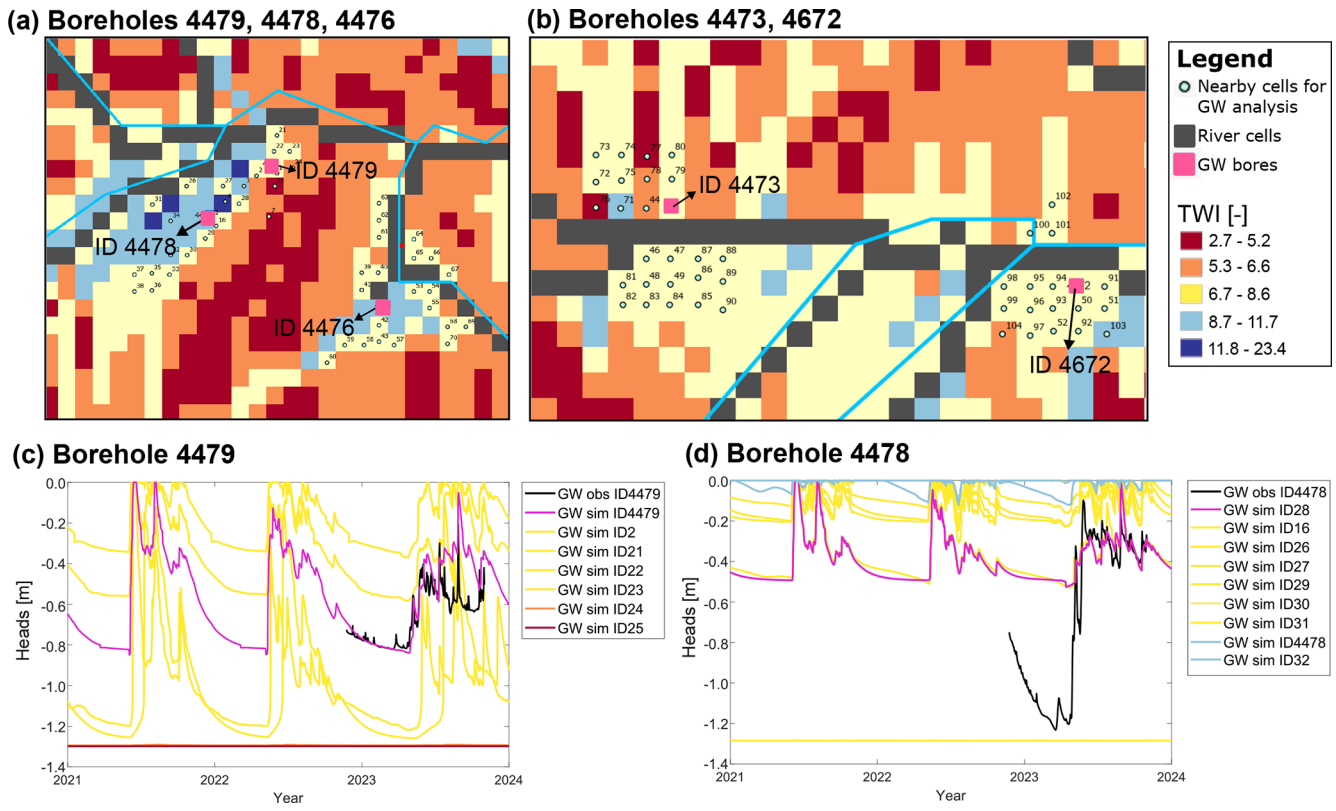

Figure 5. Spatial distribution of the Topographic Wetness Index (TWI) in the upper headwater Subcatchments (S7–S9) and the observed and simulated groundwater levels at monitored boreholes and nearby locations. **(a–b)** TWI maps (25 m × 25 m resolution) showing the five boreholes (IDs 4479, 4478, 4476, 4473, and 4672), observed river channels (blue), computed river networks (black) from *Tanalys* (Schulla, 2024), and nearby simulation locations (little dots with IDs). **(c–d)** Observed and simulated groundwater hydrographs (2021–2023) for boreholes 4479 and 4478. Black lines indicate observations, violet lines indicate the best-matching simulations (TWI ≈ 7), and the remaining colored lines represent simulations at nearby locations grouped by TWI category (red → yellow → blue). Plots of boreholes 4476, 4473, and 4672 are shown in Fig. S14 in the Supplement.

observed river water levels with a rating curve (Hofmeister et al., 2023b) where the high flows are typically underrepresented in the measurements (Di Baldassarre and Montanari, 2009).

The catchment outlet is located in the downstream Subcatchment S2. Despite the irregular observations at this station (ID 450499), the simulation captures the observed discharge dynamics (Spearman's rank correlation coefficient: 0.87 with a p-value < 0.001, NSE: 0.50, MAE: 1.50 $m^3 s^{-1}$, RMSE: 1.89 $m^3 s^{-1}$, see Figs. 6c and S2a in the Supplement). The relatively lower model performance at this downstream subcatchment (S2) compared to the other two subcatchments (S7, S8) could be because the majority of the hydrological stations that are used to calibrate the model parameters are located in the upper subcatchments. We cannot further comment on winter model performance for this station due to little reference data.

Figure 7 shows the simulated surface runoff, groundwater baseflow, and the proportion of baseflow in the streamflow in the upper headwater Subcatchments (S7, S8) and the downstream catchment outlet (Fig. 1). Following calibration against observed groundwater heads at the five piezometers, the interflow is constrained to zero (Sect. S4 and Figs. S9–S13 in the Supplements). Both surface runoff and baseflow exhibit interannual and seasonal variability and respond quickly to the peak snowmelt (Fig. 7a–f). The surface runoff shows to dominate the total discharge in the subcatchments (Fig. 7a–c). The relative low baseflow might be attributed to the piezometers being installed exclusively in the upper headwater subcatchments with shallow soil formation (Ramskogler et al., 2023), where the baseflow contribution is likely smaller than the area with thick soil profile such as the valley floor (see Fig. 1 in the work of van Tiel et al. (2024)). Besides this, a small hydraulic gradient between groundwater table and river was observed in the field (i.e., shallow river depths < 10 cm and river width < 2 m in the flat flood plain where the hydro(geo)logical stations are installed, see Fig. 1d), leading to lower groundwater exfiltration to the river. Furthermore, given that only shallow groundwater heads are measured in this study, the quantified baseflow pri-

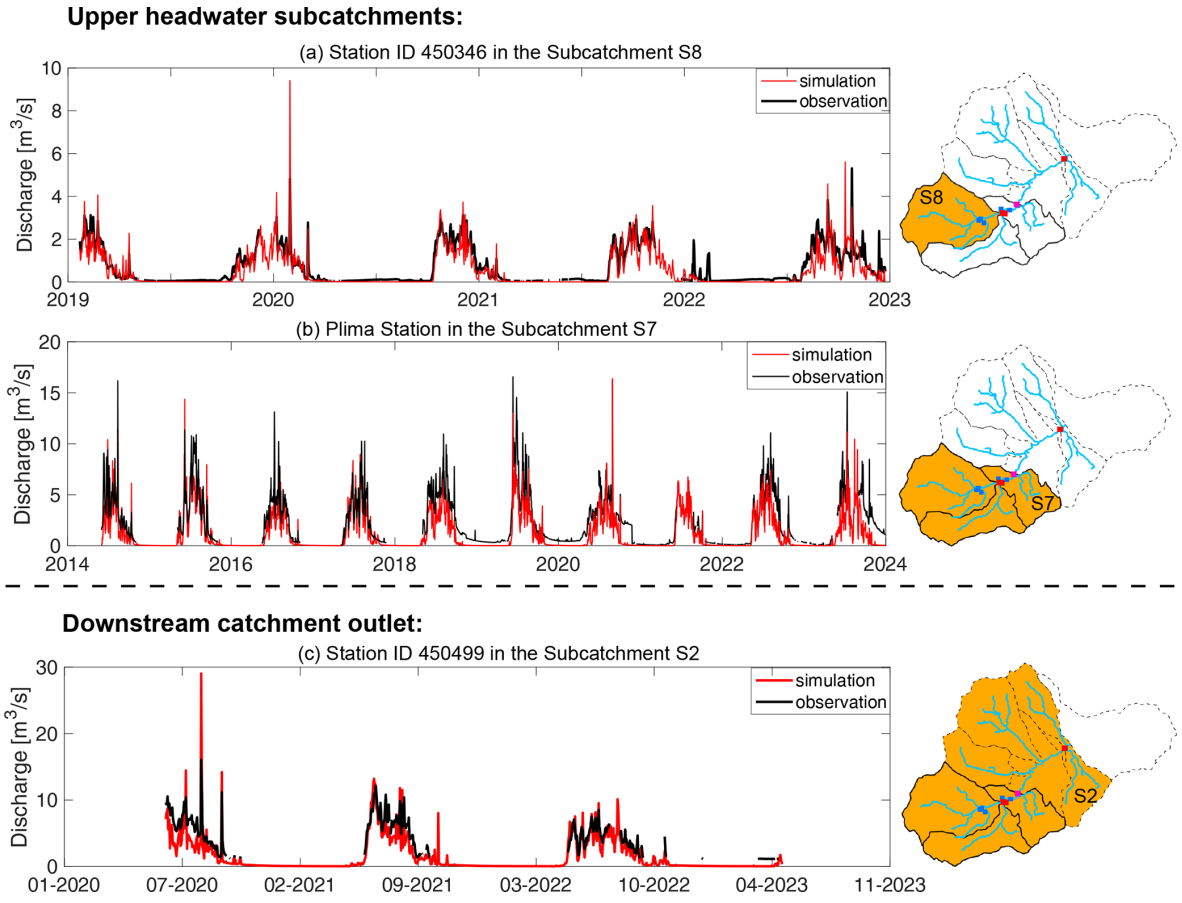

Figure 6. Observed and simulated river discharge at **(a)** Station ID 450346 located in the upper headwater Subcatchment S8, **(b)** Plima Station located in the upper headwater Subcatchment S7, and **(c)** Station ID 450499 located in the Subcatchment S2 and measuring the downstream catchment outlet. The black lines denote the observations, and the red lines denote the simulations. The drainage area of each gauging station is marked in orange in the maps on the right. The dark blue dots denote the groundwater piezometers; the red dots denote the river gauges. Details of the hydro(geo)logical stations are provided in Fig. 1 and Table 2.

marily represents the contribution from unconfined shallow aquifers. The estimated downstream baseflow (Fig. 7i) may contain higher uncertainty due to lack of deep groundwater observations and should be interpreted with caution.

Nevertheless, excluding deep groundwater from the model does not compromise the model's merit in the headwater catchment scale. Results show that shallow aquifers contribute significantly to sustaining winter streamflow: up to 30 %–40 % in the upper headwater subcatchments (S7, S8) – similar magnitude to the proglacial outwash plain in the Swiss Alps (Fig. 13 in the work of Müller et al., 2022). During the snow accumulation period, the model reproduces the observed groundwater level decline reasonably well for borehole ID 4479 but underestimates it for borehole ID 4478 (Fig. 4a, b), indicating that shallow aquifers described in the model may locally overestimate the storage (Fig. 4a, b). However, the shallow piezometers do not fall dry, and the experimental evidence does not preclude connectivity between the shallow aquifer and the river during this period. The stable water isotope analyses from November 2022 and November 2023 show consistent values between shallow groundwater and river water during the onset of low flow season (e.g., δ^2H: −94 ‰, −96 ‰, −90 ‰ at boreholes ID 4478, ID 4479, and stream gauge ID 450346 in November 2022; −85 ‰ at both borehole ID 4478 and the stream gauge ID 450346 in November 2023), despite the uncertainty due to a limited number of water samples. These results further support the hypothesis of a tight connection between the shallow aquifer and the river during winter.

5.5 Spatial analysis of key hydrological dynamics

Figures 8 and 9 show the simulated key hydrological spatial dynamics of monthly percolation, groundwater recharge, groundwater heads, groundwater exfiltration to the river, and river infiltration into the groundwater in February (lowest flow), June (peak snowmelt), September, and December (low flow) 2023. The regions marked with dashed squares (i.e., Subcatchments S7–S9 in Fig. 1) have the majority of

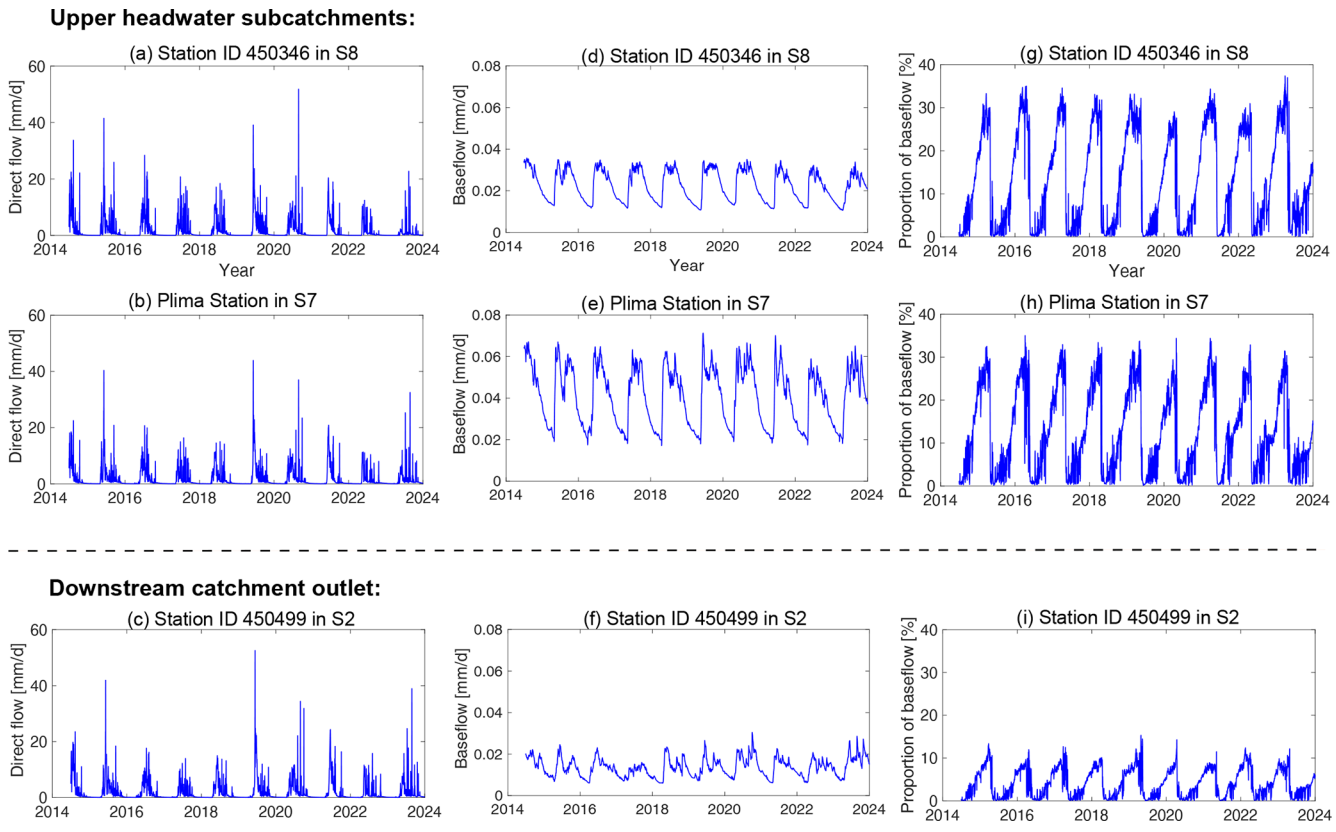

Figure 7. Simulated surface runoff (direct flow), baseflow, and the proportion of baseflow in the streamflow in the upper headwater Subcatchments (S7, S8) and the downstream catchment outlet (located in Subcatchment S2). **(a–c)** Direct flow in mm d^{-1}, **(d–f)** baseflow in mm d^{-1}, **(g–i)** the proportion of baseflow [%] in the streamflow. Note that following the calibration to the observed groundwater heads, the interflow was constrained to zero. The locations of the subcatchments are shown in Fig. 1.

hydro(geo)logical stations installed, with which the model was calibrated. The groundwater patterns shown outside the Subcatchments S7–S9 should hence be interpreted as exploratory spatial model outputs based on the transferred subsurface parameterization. Percolation represents the vertical free drainage into the groundwater. The groundwater recharge is calculated as the water balance between the vertical and horizontal inflow and outflow for each grid cell. During the low flow period in February 2023, percolation and groundwater recharge were minimal across the catchment. The groundwater heads lay within 1 m depth near the river networks and the Zufritt lake in winter, whereas they dropped beyond the model's lower boundary in other regions (Fig. 8). During the peak snowmelt period around May and June, percolation reached its annual maximum, leading to widespread groundwater recharge across the catchment–except at very high elevations and in steep terrain (Fig. 8). Consequently, groundwater levels rose, particularly near river channels and in valley bottoms. The percolation, recharge, and groundwater heads remained at a high level until September 2023, when the total liquid input (rainfall, snowmelt, glacier melt) into the catchment was still high (Fig. 3b). After that, they gradually turned to a low state in December 2023.

Figure 9 illustrates the seasonal spatial dynamics of groundwater-river interactions. Groundwater consistently exfiltrates to the river throughout the year in the main river channels, meaning these reaches behave as "gaining streams", with exfiltration rates decreasing as elevation increases. Groundwater is found to recharge the river channels even at the highest elevations during peak snowmelt (in June), when the stream network is fully developed and gaining-stream conditions extend across the network. In contrast, in February, groundwater only recharges the main river channels, and gaining-stream conditions become spatially restricted as groundwater exfiltration becomes disconnected in river networks at higher elevations, where parts of the stream network are inactive. This is in line with the typically observed retraction of the stream networks during winter months at comparable elevations (Michel et al., 2022; Paillex et al., 2020). Unlike groundwater exfiltration, river infiltration into groundwater (i.e., "losing-stream" conditions) occurs only in the main river channels at the valley bottom. This is because baseflow (groundwater exfiltration) can occur at any river cell adjacent to a groundwater cell, while river infiltration into groundwater is limited to the groundwater cells adjacent to the main river channels in *WaSiM*. This setup re-

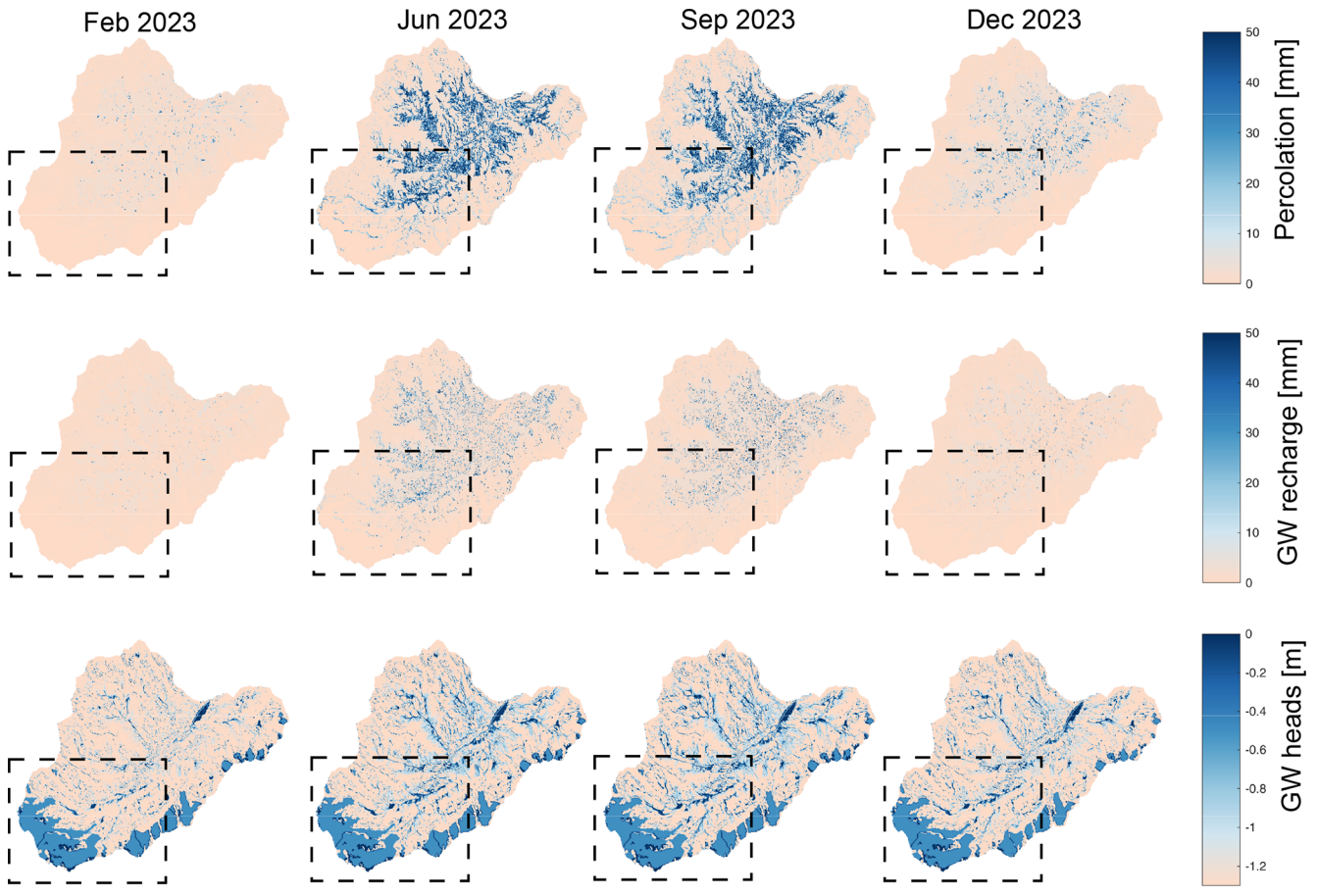

Figure 8. Spatial distribution of simulated monthly percolation, groundwater recharge, and groundwater heads (in depth to water table) in the Martell Valley in February, June, September, and December 2023. The "Percolation" is defined as the vertical flux into the groundwater system, while the "groundwater recharge" is defined as the net change of groundwater storage after balancing both vertical and horizontal inflow and outflow in the *WaSiM* model. The dashed squares indicate the area containing the majority of installed hydro(geo)logical stations (i.e., Subcatchments S7–S9 in Fig. 1), where the results have higher confidence.

flects the assumption in the model that flow gradient is usually directed from groundwater to rivers in the headwater landscapes, with reversal of this gradient - and thus the formation of losing streams– only possible under large external inflows to the routing channels (Schulla, 2024). It is worth noting that the seasonal patterns reported here reflect temporal variations in flux activity along the prescribed stream network, which remains fixed in the simulation (Sect. 6.4).

6 Discussion

6.1 Comparison with existing modeling efforts

Our results can be compared most directly with those of Thornton et al. (2022), who externally coupled *WaSiM* (surface module) (Schulla, 2024, 1997) and *HydroGeoSphere* (HGS, subsurface module) (Aquanty, 2016) to investigate groundwater-surface water interactions in a high Alpine catchment. Thornton et al. (2022) emphasized the importance of the near-surface soil zone for partitioning rainfall and meltwater between surface and subsurface pathways. By adopting a fully-integrated modeling approach, our results support the importance of this partitioning process as well, by including groundwater observations to provide additional constraints on the modelled water fluxes. Additionally, the fully-integrated *WaSiM* model adopted in our study reproduced both shallow groundwater dynamics and streamflow with comparatively limited hydrogeological information, although the simplified structure assumptions should be kept in mind, including the model requirement that the lower boundary of the soil profile corresponds to the lower boundary of the aquifer, which may limit its applicability in catchments with more complex subsurface structure. Conversely, the physically more detailed three-dimensional HGS model requires a substantially greater degree of calibration effort and (hydro)geological data, which are often unavailable in high-elevation glacierized catchments. The relative performance of the two approaches (e.g., Figs. 3 and 4 in the works

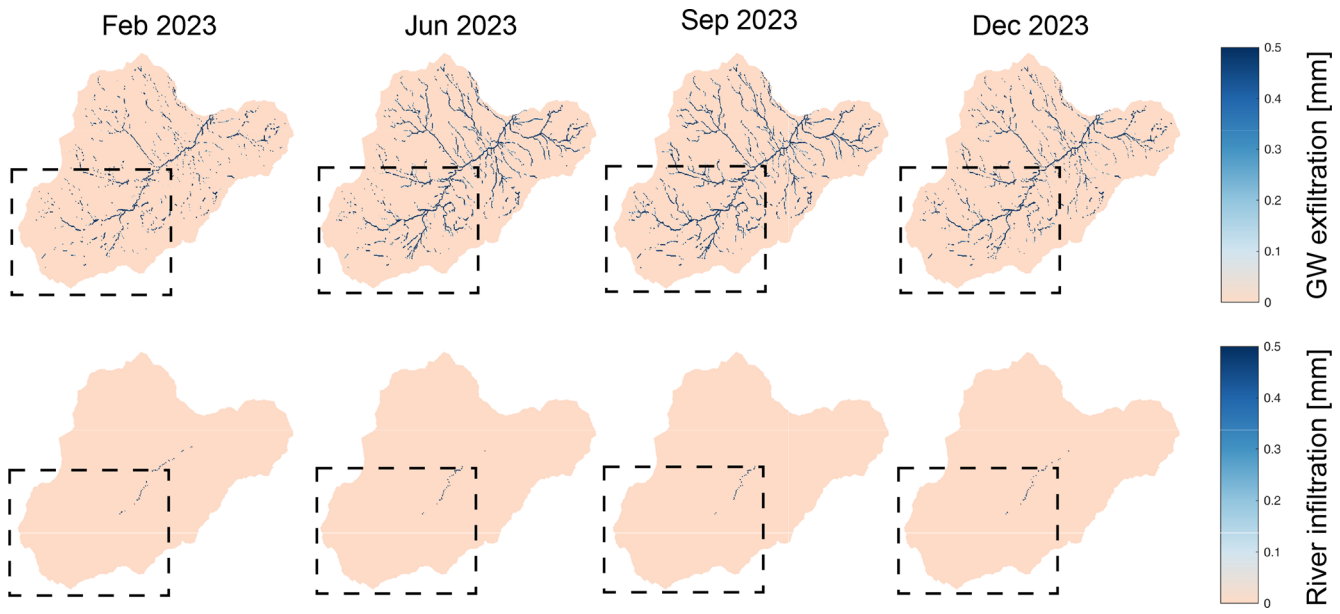

Figure 9. Interactions between groundwater and river networks (groundwater exfiltration to the river, river infiltration into groundwater) in the Martell Valley in February, June, September, and December 2023. The dashed squares indicate the area containing the majority of installed hydro(geo)logical stations (i.e., Subcatchments S7–S9 in Fig. 1), where the results have higher confidence.

of Thornton et al. (2022) compared with Figs. 4 and 6 in this work) suggests that intermediate-complexity integrated models (e.g., *WaSiM*) may provide a useful compromise for process-based modelling in data-limited high Alpine environments.

Our findings also contribute to the growing body of work evaluating groundwater–cryosphere interactions using groundwater observations. Aubry-Wake et al. (2024) demonstrated the value of shallow groundwater level data for quantifying hydrological processes in high Alpine catchments, and van Tiel et al. (2024) highlighted the broader challenges associated with representing groundwater dynamics in cryospheric environments. In line with these studies, our study shows that the inclusion of groundwater observations provided information that could not be inferred from streamflow alone. In particular, the groundwater data indicate that satisfactory streamflow simulations do not necessarily imply a realistic representation of subsurface processes. This finding reinforces the importance of multi-variate evaluation frameworks when assessing hydrological model performance.

Finally, our results are consistent with recent studies that advocate incorporating subsurface information into model calibration and evaluation (Liu et al., 2025; Talbot et al., 2024). In catchments where groundwater observations are unavailable, groundwater recharge estimates have been proposed as alternative constraints for improving the representation of surface–subsurface interactions (Liu et al., 2025). Although such estimates are generally associated with larger uncertainties than groundwater level observations, they contribute to improved quantification of internal hydrological fluxes and to reducing equifinality during model calibration. Together, these studies and our results demonstrate that incorporating subsurface information is crucial for evaluating model realism and improving process understanding in glacierized catchments.

6.2 Insights from fully-integrated hydrological modeling

The observations of shallow groundwater heads reveal rapid responses to peak melt and extreme rainfall events, with dynamics comparable to streamflow fluctuations (Fig. 3). This rapid response is consistent with runoff generation involving groundwater feedback mechanisms (Ala-aho et al., 2017; Appels et al., 2017) and highlights the importance of explicitly constraining subsurface dynamics in hydrological models. Physically based models can potentially capture rapid shallow groundwater responses to peak melt and extreme rainfall events when the relevant flow pathways are adequately represented through model structure, parameterization, spatial discretization, and boundary conditions. In the present *WaSiM* application, a particular advantage is the integrated representation of surface runoff, unsaturated-zone lateral flow, shallow groundwater dynamics, and groundwater-streamflow exchange within the same fully-distributed framework. This structure enables the relative contribution of these flow components to be evaluated jointly against both groundwater head and streamflow observations. The resulting simulations therefore contribute to investigating the processes and mechanisms that govern

surface water-groundwater interactions in the high Alpine catchment. An additional feature of *WaSiM* relevant to this study is its groundwater module, which provides a physics-based representation of groundwater dynamics within the integrated modeling framework. This differs from some other distributed hydrological models, such as T&C model (Fatichi et al., 2012), where drainage from the soil is transferred directly to the stream, and mHM model (Kumar et al., 2013) and THREW-T model (Nan et al., 2025), where groundwater dynamics are represented using conceptual linear stores.

Another key outcome of our analysis is that the daily streamflow and shallow groundwater dynamics can be reproduced without requiring the *WaSiM* interflow component (Figs. 4 and S9–S13 in the Supplement). Importantly, it highlights the need to calibrate hydrological models against observations of both streamflow (flux) and groundwater dynamics (storage) to better constrain internal hydrological processes. This result highlights a model-based constraint on the representation of unsaturated-zone flow pathways in fully-distributed hydrological modeling. Nevertheless, as the Richard's equations are adopted to solve the unsaturated zone matrix flow, the lateral flow in high Alpine terrain may occur through preferential pathways that are not explicitly represented in the model setup, such as fractured-rock pathways and local perched systems.

This result further motivates the hypothesis that the contribution of subsurface lateral flow to catchment-scale daily discharge might be limited in some high Alpine catchments. Based on the physical characteristics, the alpine environments are characterized by steep slopes and are assumed to have strong contrasts in subsurface hydraulic conductivity - conditions that tend to promote subsurface lateral flow (McGuire et al., 2024). However, our study site is also characterized with shallow soils, i.e., limited storage potential, that favor percolation to aquifers which in turn can be highly connected to the stream network and show high dynamics (Hayashi, 2019). In addition, recent evidence of high erosion potential near the Zufallferner within the study site (Altmann et al., 2025) provides indirect support for the importance of surface-dominated flow pathways during rainfall and melt events. This hypothesis is further supported by the conceptual description of hydrological flow processes in high Alpine landscapes (van Tiel et al., 2024) (Fig. 1) and the highly dynamic alpine aquifer systems where the hydraulically active zones greatly contribute to streamflow (McGuire et al., 2024; Somers and McKenzie, 2020). Nevertheless, the physical relevance of this model-based result requires independent field-based testing, such as hillslope piezometer transects, distributed soil moisture measurements, tracer observations, or geophysical methods (Xie et al., 2024; Müller et al., 2022; Glaser et al., 2018). As reviewed by McGuire et al. (2024), observing subsurface lateral flow in high Alpine catchments remains a considerable challenge. The limited availability of observational data has substantially constrained our ability to accurately predict subsurface lateral flow and quantify its contribution to streamflow across diverse hydrological settings.

6.3 Recommendations on groundwater piezometer installation and evaluation

By calibrating the subsurface module against observed groundwater heads, we found that the model performance varies among piezometer locations, indicating the challenges of representing local hydrogeological conditions in fully-distributed hydrological models. Based on these results, we suggest the following considerations for future groundwater monitoring and model evaluation in high-elevation catchments.

(i) We recommend considering the Topographic Wetness Index (TWI) as one important criterion when designing piezometer networks. TWI provides spatially explicit information on topographic controls on wetness and can therefore help stratify groundwater observations across contrasting hydro-topographic settings. It can potentially be used to ensure that monitoring captures a representative range of topographically controlled wetness conditions across the catchment. Importantly, TWI should be considered together with other site characteristics, including hydrogeology, geomorphology, soil properties, proximity to the stream network, accessibility, and the objectives of the monitoring campaign. In this framework, TWI provides a practical and readily available primary information when selecting piezometer locations in data-scarce high Alpine environments. In addition, an iterative monitoring design informed by preliminary model simulations could be a useful strategy, particularly given that such model-guided planning has not yet been routinely incorporated into field campaign design.

(ii) For comparison between point-scale groundwater observations and distributed model simulations, we recommend evaluating an ensemble of simulations of neighbouring cells around each piezometer instead of relying on a single model grid cell (at the borehole coordinates). At a given model spatial resolution, local differences in DEM representation, channel position, spatial discretization, and observation location can lead to variations among neighbouring simulated groundwater hydrographs, whereas the median and spread (Fig. S14) potentially allow for characterizing the spatial-support uncertainty. Overall, we find that the neighbourhood statistics provide the primary measure of representativeness uncertainty, while visually examining individual simulations is crucial for interpreting local model behaviour, given that the strong local topographic heterogeneity in high Alpine catchment can produce markedly different groundwater responses over short distances (Fig. 5c, d).

6.4 Limitations

This study is among the first fully-integrated and fully-distributed hydrological modeling for a comparable high

alpine glaciated catchment, with a multi-signal calibration approach including groundwater level observations. The model is calibrated based on expert knowledge, systematic and step-by-step hand-tuning, and Monte-Carlo parametric analysis (Sects. S3 and S4 in the Supplement). Unfortunately, the automatic calibration is computationally prohibitive and the number of parameters to calibrate in the model would not align with the amount of available reference data for such an automatic calibration. Considering the parameter uncertainty, the retained calibration in this study corresponds to a physically reasonable parameterization but not to any sort of optimal parameterization. To overcome the shortcomings of calibration (e.g., inefficiency, subjective parameter choices), we tackle this challenge by following a standardized approach outlined in Sect. 4.4.2. Overall, the detailed model evaluations module by module with the observed data (SWE, annual glacier mass balance, river discharge, groundwater heads) show reasonable model performance. The relative contribution of baseflow in streamflow and the temporal and spatial interactions between surface and subsurface variables support the plausibility of the simulated system dynamics.

As the subsurface properties are calibrated against the observed groundwater heads in the upper subcatchments, the simulated baseflow in the downstream may contain higher uncertainty. Likely attributed to the same geological units and similar water fluctuation depths at all piezometers (Fig. 1), many calibrated subsurface parameters are found to be identical at the observed locations (Table 4). We include the essential subsurface heterogeneity by calibrating hydraulic conductivity for each soil layer (vertical heterogeneity) and each soil type (horizontal heterogeneity), primarily because obtaining effective (calibrated) hydraulic conductivity is a prerequisite for a hydrologic model to reliably simulate observed streamflow. It is still a key challenge in physics-based models, which often rely on pedotransfer functions to estimate hydraulic conductivity (Paschalis et al., 2022). Assigning spatially heterogeneous subsurface properties in the ungauged area involves numerous assumptions. We therefore applied a conservative approach to ensure the essential subsurface heterogeneity. Heterogeneities occurring at fine scale (e.g., soil properties and varying depths) are challenging to be characterized, as demonstrated by the vast literature in stochastic hydrogeology, starting from the detailed investigation of the famous sites of Borden and Columbus (Rehfeldt et al., 1992; Woodbury and Sudicky, 1991). Detailed exploration of the impact of spatially variable subsurface parameters is beyond the scope of this study.

These limitations are particularly relevant for the interpretation of the catchment-wide groundwater results. The groundwater observations are concentrated in Subcatchments S7–S9, where the subsurface parameters were calibrated, whereas the same parameterization was transferred to the ungauged parts of the catchment. The mapped patterns of groundwater recharge, heads, exfiltration, and infiltration outside these upper subcatchments (Figs. 8–9) should therefore be viewed mainly as exploratory model outputs. The present setup is consequently better constrained for shallow groundwater-surface water interactions, while deeper groundwater flow paths remain uncertain and would require additional observations.

As pointed out by van Tiel et al. (2024), it is challenging to describe processes controlling cryosphere-groundwater interactions in high-alpine catchments due to a lack of observations and modeling challenges. The deep aquifers might exist in the Quaternary sediments in part of the catchment, likely in the downstream valley floors. However, details of deep aquifers are vastly unavailable in alpine landscapes. Remote sensing data offer an option to estimate groundwater storage changes. We could think of GRACE satellite data (Liu et al., 2022; Xiang et al., 2016), but the low spatial resolution (hundreds of kilometers) is often too coarse for high-elevation glaciated catchments characterized by an area commonly smaller than $100\,km^2$ (e.g. in Europe), leading to high uncertainty in the estimated groundwater storage and changes and challenge to be adopted in fully-distributed hydrological models. Another limitation of satellite-based gravimetry is the superimposition of gravity changes in glaciated high mountains; for example, the changes in mass are combined impacts due to glacier melt, seasonal snow cover, and fluctuations in subsurface storage (Voigt et al., 2021). Therefore, in-situ deep groundwater level data are still required to validate the satellite data and to calibrate the fully-integrated hydrological models. By adopting integrated hydrological modeling, our research aim is to contribute to understanding how water partitioning is shaped by the near (sub)surface hydrological processes.

Additionally, we acknowledge the hydrological simulation uncertainty due to the relatively coarse spatial resolution of the adopted soil dataset (HWSD, $1\,km \times 1\,km$), which is primarily limited by the sparse field observations available in the high mountain environments. A slightly higher resolution of global soil product (e.g., SoliGrids in $250\,m \times 250\,m$) (Batjes et al., 2020) may not necessarily improve the simulations significantly because of limited field observations in the high elevations. In this study, we used the land use map (e.g., the presence of rocks, forests, and grasslands) to evaluate and modify the soil type data, as another layer of validation of data quality. The HWSD product is adopted in this study as it remains widely used in regional modeling (Trinh et al., 2018; Bosco et al., 2015; Livneh et al., 2015) and it has harmonized and internally consistent soil attributes across broad spatial extents.

In the highest part of the Martell Valley, permafrost might exist, where water from snowmelt, ice melt, and rainfall may undergo multiple freeze-thaw cycles under periglacial conditions before entering the aquifers and being discharged (Brighenti et al., 2023; Reato et al., 2022). However, permafrost-related freezing and thawing processes are not included in our simulations, given that the corresponding

WaSiM parameters could not be reliably constrained without soil temperature observations. Although the model can simulate soil freezing and thawing, spatially-distributed soil temperature measurements are needed for calibration and evaluation of freezing and thawing depths, but such observations are rarely available in high-elevation catchments. We acknowledge that in regions with significant glacier and permafrost cover, neglecting these effects may introduce uncertainty in characterizing groundwater components, with potential shortcomings in snow and ice melt estimates.

Another structural assumption is the fixed representation of the stream network. In the present *WaSiM* setup, stream cells are prescribed from the DEM and remain static. As the stream networks in high-elevation headwaters can be dynamic, this assumption may influence the simulated spatial extent of groundwater-streamflow exchange. The seasonal variability (Figs. 8–9) should therefore be interpreted as changes in hydrological fluxes along this potential channel network. Furthermore, dynamically updating drainage networks in distributed models remains highly challenging, given that changes in channel topology require continuous updates of spatial model structure and state variables. This issue is particularly relevant in glacierized environments, where landscape evolution can alter drainage pathways. Fan et al. (2026b) highlight updating stream networks after glacier retreat as a key challenge for non-stationary distributed hydrological modeling. Future model developments enabling dynamic updating of stream cells will improve the representation of groundwater-surface water interactions in high Alpine catchments.

7 Conclusions

In this study, we simulate the complex surface-subsurface hydrological processes and quantify the interactions between the key hydrological components (snowmelt, glacier melt, river discharge, groundwater) in a high-elevation glaciated catchment (Martell Valley) with the fully-integrated and fully-distributed hydrological model *WaSiM*. Results show that the shallow groundwater heads respond as quickly as streamflow to peak snowmelt and extreme rainfall events (Fig. 3), indicating the need for improved subsurface parametrization in high Alpine hydrological modeling. By incorporating shallow groundwater heads into the multi-signal calibration, we find that the daily dynamics of streamflow and shallow groundwater level can be reproduced without requiring the *WaSiM* interflow component, highlighting a model-based constraint on representing unsaturated-zone flow pathways in fully-distributed modeling. This study also underscores the crucial contribution of winter groundwater baseflow to streamflow in high-elevation Alpine catchments and the dynamic temporal and spatial interactions between surface water and groundwater.

Furthermore, the results underline the challenges of integrating point-scale groundwater observations into the calibration of a fully-distributed hydrological model. To overcome such challenges, we recommend considering the Topographic Wetness Index (TWI) as one important criterion when designing piezometer networks. TWI provides spatially explicit information on topographic controls on wetness and can therefore help stratify groundwater observations across contrasting hydro-topographic settings. Together with other field information and the objectives of the monitoring campaigns, TWI provides a practical and readily available primary information when selecting piezometer locations in data-scarce high Alpine environments. Additionally, we recommend evaluating the simulated ensemble of groundwater hydrographs from a range of neighboring cells near the observed locations to address the intrinsic observational and modeling uncertainties.

As one of the first fully-distributed and fully-integrated surface-subsurface hydrological modeling studies in the high-elevation glaciated environment, the achieved observational and modeling insights should be further tested and confirmed in other high Alpine settings. The insights from this study are most likely applicable to the mountain ranges with similar climatic, geological, and landscape settings and the sites with similar subsurface properties, such as the central European Alps, Scandinavian Mountains, and Canadian Rockies (Welch and Shaw, 2025; Stutenbecker et al., 2016; Ebbing et al., 2012). The high-elevation headwater catchments in these non-carbonate mountain ranges share key characteristics, where Quaternary sediments host shallow aquifers and impermeable bedrock restricts deep percolation. These are opposed to settings with distinct subsurface properties, e.g. the Hindu Kush Himalaya or with very different climatic settings, e.g. the Andean Alps (Owen and Dortch, 2014; Duncan et al., 2003). Future investigations can refer to the demonstrated workflow and recommendations (Sect. 6.3) and potentially overcome the limitations (Sect. 6.4). Such global case modeling and intercomparison contribute to a holistic understanding of hydrological processes in high Alpine environments.

Code availability. A compiled version of the hydrological model *WaSiM* is available at http://www.wasim.ch/en/ (last access: 5 August 2024) (no source code available) (Schulla, 2024). The ΔSnow model (v1.0.2) used for transforming the snow height data to snow water equivalent is accessible in the R package "*niXmass*" (https://doi.org/10.5194/hess-25-1165-2021, Winkler et al., 2021). The MATLAB function *mannkendall* (v1.0.0) is adopted for quantifying the temporal trends of the hydrological variables (https://doi.org/10.5281/zenodo.4495589, Collaud Coen and Vogt, 2021; https://doi.org/10.5194/amt-13-6945-2020, Collaud Coen et al., 2020).

Data availability. The hydro-meteorological data used in this study are available in Zenodo (https://doi.org/10.5281/zenodo.21246869; Fan et al., 2026a). The river gauge ID 450499 was destroyed during the extreme flooding events between 12 July and 9 August 2023. The discharge data of the official Plima Station are obtained from the Autonomous Province of Bozen (Bolzano) – South Tyrol. The observed climate data at Station Langenferner are obtained from the Institute of Atmospheric and Cryospheric Sciences of the University of Innsbruck in Austria. The data at Station Careser are obtained from Meteo Trentino in Italy (http://storico.meteotrentino.it/web.htm?ppbm=T0065&rs&1&df, last access: 15 February 2024). Other station data are obtained from the Autonomous Province of Bolzano, South Tyrol in Italy. The Digital Elevation Model (DEM) data in 2006 are obtained from Province of Bolzano (di Bolzano Alto Adige, 2006). The land use and land cover data of the site in 2018 are obtained from the Corine Land Cover Data Center (CORINE Land Cover, 2018). The soil profile and attributes in 2018 are extracted from the Harmonized World Soil Database (version 2.0) (FAO and IIASA, 2023; https://doi.org/10.5194/bg-20-2919-2023, Ramskogler et al., 2023). The geological information of the site is obtained from the map produced by Berra et al. (2012). The glacier coverage maps of the site are obtained from Knoflach et al. (2021) (https://doi.org/10.3390/rs13214450).

Supplement. The supplement related to this article is available online at https://doi.org/10.5194/hess-30-7197-2026-supplement.

Author contributions. All authors participated in the conceptualization, methodology, data acquisition, design of the experiment, and discussion on the results. XF carried out the formal analyses and investigations. The hydrological *WaSiM* model is calibrated by XF and FH. XF wrote the original manuscript and visualized all the results, all co-authors contributed to the editing and review. BS and GC supervised the work and acquired the project funding.

Competing interests. The contact author has declared that none of the authors has any competing interests.

Disclaimer. Publisher's note: Copernicus Publications remains neutral with regard to jurisdictional claims made in the text, published maps, institutional affiliations, or any other geographical representation in this paper. The authors bear the ultimate responsibility for providing appropriate place names. Views expressed in the text are those of the authors and do not necessarily reflect the views of the publisher.

Acknowledgements. We acknowledge the valuable discussions about the hydrological modeling results with the *WaSiM* developer Jörg Schulla. We thank the technician Mr. Michael Tarantik and the students at the Technical University of Munich for measuring and obtaining the hydrological data in the Martell Valley. We thank Dr. Natalie Ceperley at University of Bern for the laboratory analysis of the stable water isotopes. We thank the project partners in Eurac Italy for providing the information on the catchment land cover, geology, and soil properties, also thank the official authorities of Autonomous Province of Bolzano in South Tyrol, Institute of Atmospheric and Cryospheric Sciences of the University of Innsbruck, Meteo Trentino in Italy for providing the research data. XF, FH, and GC acknowledge the support of the German Research Foundation (DFG) research unit (FOR2793/2) investigating the "Sensitivity of High Alpine Geosystems to Climate Change since 1850" (SEHAG) under grant CH981/3-2. XF and BS acknowledge the Swiss National Science Foundation (SNSF) grant (200020E-204030) for "SEHAG Subproject 2 -Impact of climate change on groundwater storage in high Alpine catchments: from observation to model predictions".

Financial support. This research has been supported by the NAME OF FUNDER (grant no. GRANT AGREEMENT NO).

Review statement. This paper was edited by Nunzio Romano and reviewed by four anonymous referees.

References

Abhervé, R., Roques, C., Gauvain, A., Longuevergne, L., Louaisil, S., Aquilina, L., and de Dreuzy, J.-R.: Calibration of groundwater seepage against the spatial distribution of the stream network to assess catchment-scale hydraulic properties, Hydrol. Earth Syst. Sci., 27, 3221–3239, https://doi.org/10.5194/hess-27-3221-2023, 2023.

Ala-aho, P., Soulsby, C., Wang, H., and Tetzlaff, D.: Integrated surface-subsurface model to investigate the role of groundwater in headwater catchment runoff generation: A minimalist approach to parameterisation, J. Hydrol., 547, 664–677, https://doi.org/10.1016/j.jhydrol.2017.02.023, 2017.

Altmann, M., Fischer, P., Haas, F., Pfeiffer, M., Ramskogler, K., Rom, J., Kara-Timmermann, D., Himmelstoß, T., Heckmann, T., and Becht, M.: Simulation of soil erosion in the Little Ice Age glacier foreland of the Zufallferner (South Tyrol, Italy) using Erosion-3D, EGU General Assembly 2025, Vienna, Austria, 27 Apr–2 May 2025, EGU25-5734, https://doi.org/10.5194/egusphere-egu25-5734, 2025.

Appels, W. M., Bogaart, P. W., and van der Zee, S. E.: Feedbacks between shallow groundwater dynamics and surface topography on runoff generation in flat fields, Water Resour. Res., 53, 10336–10353, https://doi.org/10.1002/2017WR020727, 2017.

Aquanty, I.: HydroGeoSphere user manual, https://hydrogeosphere.blob.core.windows.net/hydrogeosphere/hgs/hydrosphere_ref.pdf (last access: 15 February 2024), 2016.

Arnoux, M., Brunner, P., Schaefli, B., Mott, R., Cochand, F., and Hunkeler, D.: Low-flow behavior of alpine catchments with varying quaternary cover under current and future climatic conditions, J. Hydrol., 592, 125591, https://doi.org/10.1016/j.jhydrol.2020.125591, 2021.

Aubry-Wake, C., McNamara, G., Somers, L. D., McKenzie, J. M., Pomeroy, J. W., and Hellström, R.: Sensitivity of surface water and groundwater contributions to streamflow in a tropical glacierized basin under climate change scenarios, Environ. Res.

Lett., 19, 114036, https://doi.org/10.1088/1748-9326/ad7c68, 2024.

Autonome Province of Bolzano: Vedretta Lunga Langenferner, Glacier report, 142, https://assets-eu-01.kc-usercontent.com/53721173-39bb-0184-4b45-ca96e975b8d7/7e806ed1-a48e-4da5-96ce-a67521282f2b/pr186428_glacierreport_022009.pdf (last access: 15 June 2024), 2007.

Avanzi, F., Munerol, F., Milelli, M., Gabellani, S., Massari, C., Girotto, M., Cremonese, E., Galvagno, M., Bruno, G., Morra di Cella, U., Rossi, L., Altamura, M., and Ferraris, L.: Winter snow deficit was a harbinger of summer 2022 socio-hydrologic drought in the Po Basin, Italy, Commun. Earth Environ., 5, 64, https://doi.org/10.1038/s43247-024-01222-z, 2024.

Bahr, D. B., Meier, M. F., and Peckham, S. D.: The physical basis of glacier volume-area scaling, J. Geophys. Res.: Solid Earth, 102, 20355–20362, https://doi.org/10.1029/97JB01696, 1997.

Bahr, D. B., Pfeffer, W. T., and Kaser, G.: A review of volume-area scaling of glaciers, Rev. Geophys., 53, 95–140, https://doi.org/10.1002/2014RG000470, 2015.

Banerjee, A., Kang, S., Guo, W., Meadows, M. E., Wang, W., Sengupta, D., and Zhang, T.: Glacier retreat and lake outburst floods in the central Himalayan region from 2000 to 2022, Nat. Haz., 120, 5485–5508, https://doi.org/10.1007/s11069-024-06415-5, 2024.

Batjes, N. H., Ribeiro, E., and van Oostrum, A.: Standardised soil profile data to support global mapping and modelling (WoSIS snapshot 2019), Earth Syst. Sci. Data, 12, 299–320, https://doi.org/10.5194/essd-12-299-2020, 2020.

Berra, F., Sciesa, E., Mazoccola, D., Mair, V., Longhin, M., Gazzola, D., and Guglielmin, M.: Kartiergebiete des Grundgebirges und der Permo-Mesozoischen Sedimentabfolge im Masstab 1 : 10000, 2012.

Beven, K. J. and Kirkby, M. J.: A physically based, variable contributing area model of basin hydrology, Hydrol. Sci. J., 24, 43–69, https://doi.org/10.1080/02626667909491834, 1979.

Borzi, I.: Modeling groundwater resources in data-scarce regions for sustainable management: Methodologies and limits, Hydrology, 12, 11, https://doi.org/10.3390/hydrology12010011, 2025.

Bosco, C., de Rigo, D., Dewitte, O., Poesen, J., and Panagos, P.: Modelling soil erosion at European scale: towards harmonization and reproducibility, Nat. Hazards Earth Syst. Sci., 15, 225–245, https://doi.org/10.5194/nhess-15-225-2015, 2015.

Brighenti, S., Engel, M., Dinale, R., Tirler, W., Voto, G., and Comiti, F.: Isotopic and chemical signatures of high mountain rivers in catchments with contrasting glacier and rock glacier cover, J. Hydrol., 623, 129779, https://doi.org/10.1016/j.jhydrol.2023.129779, 2023.

Bronstert, A., Niehoff, D., and Schiffler, G. R.: Modelling infiltration and infiltration excess: The importance of fast and local processes, Hydrol. Proc., 37, e14875, https://doi.org/10.1002/hyp.14875, 2023.

Brutsaert, W.: Evaporation into the atmosphere, Kluwer Academic Publishers, Dordrecht, https://doi.org/10.1007/978-94-017-1497-6, 1982.

Carletti, F., Michel, A., Casale, F., Burri, A., Bocchiola, D., Bavay, M., and Lehning, M.: A comparison of hydrological models with different level of complexity in Alpine regions in the context of climate change, Hydrol. Earth Syst. Sci., 26, 3447–3475, https://doi.org/10.5194/hess-26-3447-2022, 2022.

Ceperley, N., Zuecco, G., Beria, H., Carturan, L., Michelon, A., Penna, D., Larsen, J., and Schaefli, B.: Seasonal snow cover decreases young water fractions in high Alpine catchments, Hydrol. Proc., 34, 4794–4813, https://doi.org/10.1002/hyp.13937, 2020.

Chen, J. and Ohmura, A.: Estimation of Alpine glacier water resources and their change since the 1870s, IAHS, 193, 127–135, 1990.

Chen, Z., Lucianetti, G., and Hartmann, A.: Understanding groundwater storage and drainage dynamics of a high mountain catchment with complex geology using a semi-distributed process-based modelling approach, J. Hydrol., 625, 130067, https://doi.org/10.1016/j.jhydrol.2023.130067, 2023.

Coderre, P., Knoben, W., Thébault, C., Vásquez, N., Clark, M., and Pietroniro, A.: The impact of benchmark selection on spatial patterns of model evaluation metrics, EGU General Assembly 2026, Vienna, Austria, 3–8 May 2026, EGU26-15343, https://doi.org/10.5194/egusphere-egu26-15343, 2026.

Collaud Coen, M. and Vogt, F. P.: mannkendall/Matlab: Bug fix: prob_mk_n (v1.1.0)., Zenodo [code], https://doi.org/10.5281/zenodo.4495589, 2021.

Collaud Coen, M., Andrews, E., Bigi, A., Martucci, G., Romanens, G., Vogt, F. P. A., and Vuilleumier, L.: Effects of the prewhitening method, the time granularity, and the time segmentation on the Mann–Kendall trend detection and the associated Sen's slope, Atmos. Meas. Tech., 13, 6945–6964, https://doi.org/10.5194/amt-13-6945-2020, 2020.

CORINE Land Cover: CORINE Land Cover Data 2018, https://land.copernicus.eu/en/products/corine-land-cover (last access: 15 February 2024), 2018.

Cornelissen, T., Diekkrüger, B., and Giertz, S.: A comparison of hydrological models for assessing the impact of land use and climate change on discharge in a tropical catchment, J. Hydrol., 498, 221–236, https://doi.org/10.1016/j.jhydrol.2013.06.016, 2013.

Di Baldassarre, G. and Montanari, A.: Uncertainty in river discharge observations: a quantitative analysis, Hydrol. Earth Syst. Sci., 13, 913–921, https://doi.org/10.5194/hess-13-913-2009, 2009.

di Bolzano Alto Adige, P. A.: Digitales Geländemodell (DGM 2.5 m), https://data.civis.bz.it/de/dataset/modello-digitale-del-terreno-dtm-25m (last access: 15 February 2024), 2006.

Dobler, C. and Pappenberger, F.: Global sensitivity analyses for a complex hydrological model applied in an Alpine watershed, Hydrol. Proc., 27, 3922–3940, https://doi.org/10.1002/hyp.9520, 2013.

Drenkhan, F., Buytaert, W., Mackay, J. D., Barrand, N. E., Hannah, D. M., and Huggel, C.: Looking beyond glaciers to understand mountain water security, Nat. Sustain., 6, 130–138, https://doi.org/10.1038/s41893-022-00996-4, 2023.

Duncan, C., Masek, J., and Fielding, E.: How steep are the Himalaya? Characteristics and implications of along-strike topographic variations, Geology, 31, 75–78, https://doi.org/10.1130/0091-7613(2003)031<0075:HSATHC>2.0.CO;2, 2003.

Dunne, T.: Relation of field studies and modeling in the prediction of storm runoff, J. Hydrol., 65, 25–48, https://doi.org/10.1016/0022-1694(83)90209-3, 1983.

Dussaillant, I., Hugonnet, R., Huss, M., Berthier, E., Bannwart, J., Paul, F., and Zemp, M.: Annual mass change of the world's glaciers from 1976 to 2024 by temporal downscaling of satellite data with in situ observations, Earth Syst. Sci. Data, 17, 1977–2006, https://doi.org/10.5194/essd-17-1977-2025, 2025.

Ebbing, J., England, R., Korja, T., Lauritsen, T., Olesen, O., Stratford, W., and Weidle, C.: Structure of the Scandes lithosphere from surface to depth, Tectonophysics, 536, 1–24, https://doi.org/10.1016/j.tecto.2012.02.016, 2012.

Engdahl, N. B.: Impacts of permeability uncertainty in a coupled surface-subsurface flow model under perturbed recharge scenarios, Water Resour. Res., 60, e2023WR035975, https://doi.org/10.1029/2023WR035975, 2024.

Fan, X., Goeppert, N., and Goldscheider, N.: Quantifying the historic and future response of karst spring discharge to climate variability and change at a snow-influenced temperate catchment in central Europe, Hydrogeol. J., 31, 2213–2229, https://doi.org/10.1007/s10040-023-02703-9, 2023a.

Fan, X., Peterson, T. J., Henley, B. J., and Arora, M.: Groundwater sensitivity to climate variations across Australia, Water Resour. Res., 59, e2023WR035036, https://doi.org/10.1029/2023WR035036, 2023b.

Fan, X., Hofmeister, F., Schaefli, B., and Chiogna, G.: New insights from fully-integrated surface-subsurface hydrological modeling in high-elevation glaciated environments, Zenodo [data set], https://doi.org/10.5281/zenodo.21246869, 2026a.

Fan, X., Schaefli, B., Hofmeister, F., and Chiogna, G.: When the Past Matters: How Model Initialization Can Lead to Surprises in Long-Term Simulations in Glaciated Environments, Hydrol. Proc., 40, e70507, https://doi.org/10.1002/hyp.70507, 2026b.

FAO and IIASA: Harmonized World Soil Database Version 2.0, Rome and Laxenburg, ISRIC [data set], https://data.isric.org/geonetwork/srv/eng/catalog.search#/metadata/54aebf11-ec73-4ff8-bf6c-ecff4b0725ea (last access: 15 February 2024), 2023.

Fatichi, S., Ivanov, V. Y., and Caporali, E.: A mechanistic ecohydrological model to investigate complex interactions in cold and warm water-controlled environments: 1, Theoretical framework and plot-scale analysis, J. Adv. Model. Earth Syst., 4, M05002, https://doi.org/10.1029/2011MS000086, 2012.

Fatichi, S., Rimkus, S., Burlando, P., Bordoy, R., and Molnar, P.: High-resolution distributed analysis of climate and anthropogenic changes on the hydrology of an Alpine catchment, J. Hydrol., 525, 362–382, https://doi.org/10.1016/j.jhydrol.2015.03.036, 2015.

Förster, K., Garvelmann, J., Meißl, G., and Strasser, U.: Modelling forest snow processes with a new version of WaSiM, Hydrol. Sci. J., 63, 1540–1557, 2018.

Freudiger, D., Kohn, I., Seibert, J., Stahl, K., and Weiler, M.: Snow redistribution for the hydrological modeling of alpine catchments, Wiley Interdiscip. Rev.: Water, 4, e1232, https://doi.org/10.1002/wat2.1232, 2017.

Galos, S. P., Klug, C., Maussion, F., Covi, F., Nicholson, L., Rieg, L., Gurgiser, W., Mölg, T., and Kaser, G.: Reanalysis of a 10-year record (2004–2013) of seasonal mass balances at Langenferner/Vedretta Lunga, Ortler Alps, Italy, The Cryosphere, 11, 1417–1439, https://doi.org/10.5194/tc-11-1417-2017, 2017.

Garambois, P. A., Roux, H., Larnier, K., Castaings, W., and Dartus, D.: Characterization of process-oriented hydrologic model behavior with temporal sensitivity analysis for flash floods in Mediterranean catchments, Hydrol. Earth Syst. Sci., 17, 2305–2322, https://doi.org/10.5194/hess-17-2305-2013, 2013.

Gauthier, T. D.: Detecting trends using Spearman's rank correlation coefficient, Environ. Forens., 2, 359–362, https://doi.org/10.1006/enfo.2001.0061, 2001.

Glaser, B., Antonelli, M., Chini, M., Pfister, L., and Klaus, J.: Technical note: Mapping surface-saturation dynamics with thermal infrared imagery, Hydrol. Earth Syst. Sci., 22, 5987–6003, https://doi.org/10.5194/hess-22-5987-2018, 2018.

Grabs, T., Seibert, J., Bishop, K., and Laudon, H.: Modeling spatial patterns of saturated areas: A comparison of the topographic wetness index and a dynamic distributed model, J. Hydrol., 373, 15–23, https://doi.org/10.1016/j.jhydrol.2009.03.031, 2009.

Gruber, S.: A mass-conserving fast algorithm to parameterize gravitational transport and deposition using digital elevation models, Water Resour. Res., 43, https://doi.org/10.1029/2006WR004868, 2007.

Guyennon, N., Valt, M., Salerno, F., Petrangeli, A. B., and Romano, E.: Estimating the snow water equivalent from snow depth measurements in the Italian Alps, Cold Reg. Sci. Technol., 167, 102859, https://doi.org/10.1016/j.coldregions.2019.102859, 2019.

Hayashi, M.: Alpine hydrogeology: The critical role of groundwater in sourcing the headwaters of the world, Groundwater, 58, 498–510, https://doi.org/10.1111/gwat.12965, 2019.

Hock, R.: Modelling of glacier melt and discharge, PhD thesis, ETH Zurich, https://doi.org/10.3929/ethz-a-001891975, 1998.

Hock, R.: A distributed temperature-index ice-and snowmelt model including potential direct solar radiation, J. Glaciol., 45, 101–111, https://doi.org/10.3189/S0022143000003087, 1999.

Hofmeister, F., Arias-Rodriguez, L. F., Premier, V., Marin, C., Notarnicola, C., Disse, M., and Chiogna, G.: Intercomparison of Sentinel-2 and modelled snow cover maps in a high-elevation Alpine catchment, J. Hydrol. X, 15, 100123, https://doi.org/10.1016/j.hydroa.2022.100123, 2022.

Hofmeister, F., Graziano, F., Marcolini, G., Willems, W., Disse, M., and Chiogna, G.: Quality assessment of hydrometeorological observational data and their influence on hydrological model results in Alpine catchments, Hydrol. Sci. J., 68, 552–571, https://doi.org/10.1080/02626667.2023.2172335, 2023a.

Hofmeister, F., Venegas, B. R., Sentlinger, G., Tarantik, M., Blume, T., Disse, M., and Chiogna, G.: Automated streamflow measurements in high-elevation Alpine catchments, River Res. Appl., 39, 2079–2091, https://doi.org/10.1002/rra.4203, 2023b.

Höge, M., Kauzlaric, M., Siber, R., Schönenberger, U., Horton, P., Schwanbeck, J., Floriancic, M. G., Viviroli, D., Wilhelm, S., Sikorska-Senoner, A. E., Addor, N., Brunner, M., Pool, S., Zappa, M., and Fenicia, F.: CAMELS-CH: hydro-meteorological time series and landscape attributes for 331 catchments in hydrologic Switzerland, Earth Syst. Sci. Data, 15, 5755–5784, https://doi.org/10.5194/essd-15-5755-2023, 2023.

Horton, P., Schaefli, B., and Kauzlaric, M.: Why do we have so many different hydrological models? A review based on the case of Switzerland, Wiley Interdiscip. Rev.: Water, 9, e1574, https://doi.org/10.1002/wat2.1574, 2022.

IPCC: Climate change 2021: The Physical Science Basis. Contribution of Working Group I to the Sixth Assessment Report of the

Intergovernmental Panel on Climate Change, Cambridge University Press, https://doi.org/10.1017/9781009157896, 2021.

Isotta, F. A., Frei, C., and Schwanbeck, J.: Mean Precipitation throughout the Alps 1971–2008, in: Data and Analysis Platform, Hydrological Atlas of Switzerland, https://hydromaps.ch/#en/7/46.111/10.898/bl_hds--b02_b0200_alpine_precip_y_1971_2008v1_0$0/NULL (last access: 15 February 2024), 2018.

Jansson, P. and Karlberg, L.: Coupled heat and mass transfer model for soil-plant-atmosphere systems, Royal Institute of Technology, Dept of Civil and Environmental Engineering, Stockholm, https://www.researchgate.net/publication/304714926_Coupled_heat_and_mass_transfer_model_for_soil-plant-atmosphere_systems_Royal_Institute_of_Technology_Department_of_Civil_and_Environmental_Engineering (last access: 15 February 2024), 2004.

Jarvis, A., Reuter, H., Nelson, A., and Guevara, E.: Hole-filled seamless SRTM data V4, CGIAR-CSI [data set], http://srtm.csi.cgiar.org (last access: 15 February 2024), 2008.

Kendall, M.: Rank correlation methods, Charles Griffin, London, 196 pp., https://www.scribd.com/document/722213060/Rank-correlation-methods-Kendall-Maurice-G-Maurice-George-1907-Volume-3rd-Edition-1962-New-York-Hafner-Pub-Co-594b4db6dbaf75d161 (last access: 15 February 2024), 1962.

Knoflach, B., Ramskogler, K., Talluto, M., Hofmeister, F., Haas, F., Heckmann, T., Pfeiffer, M., Piermattei, L., Ressl, C., Wimmer, M. H., et al.: Modelling of vegetation dynamics from satellite time series to determine proglacial primary succession in the course of global warming – A case study in the upper Martell Valley (Eastern Italian Alps), Remote Sens., 13, 4450, https://doi.org/10.3390/rs13214450, 2021.

Krause, S., Bronstert, A., and Zehe, E.: Groundwater–surface water interactions in a North German lowland floodplain – implications for the river discharge dynamics and riparian water balance, J. Hydrol., 347, 404–417, https://doi.org/10.1016/j.jhydrol.2007.09.028, 2007.

Kumar, R., Samaniego, L., and Attinger, S.: Implications of distributed hydrologic model parameterization on water fluxes at multiple scales and locations, Water Resour. Res., 49, 360–379, https://doi.org/10.1029/2012WR012195, 2013.

Liu, J., Liu, J., Liu, M., Tian, S., Liu, Y., Yang, W., and Liu, Y.: Development of an alpine hydrological model considering the recharge of stream water to alluvial plain aquifers, Environmental Modelling and Software, p. 106567, https://doi.org/10.1016/j.envsoft.2025.106567, 2025.

Liu, M., Pei, H., and Shen, Y.: Evaluating dynamics of GRACE groundwater and its drought potential in Taihang Mountain Region, China, J. Hydrol., 612, 128156, https://doi.org/10.1016/j.jhydrol.2022.128156, 2022.

Livneh, B., Kumar, R., and Samaniego, L.: Influence of soil textural properties on hydrologic fluxes in the Mississippi river basin, Hydrol. Proc., 29, 4638–4655, https://doi.org/10.1002/hyp.10601, 2015.

Mann, H.: Nonparametric tests against trend, Econometrica, 13, 245–259, https://doi.org/10.2307/1907187, 1945.

Marcolini, G., Bellin, A., Disse, M., and Chiogna, G.: Variability in snow depth time series in the Adige catchment, J. Hydrol.: Reg. Stud., 13, 240–254, https://doi.org/10.1016/j.ejrh.2017.08.007, 2017.

Matiu, M., Jacob, A., and Notarnicola, C.: Daily MODIS snow cover maps for the European Alps from 2002 onwards at 250 m horizontal resolution along with a nearly cloud-free version, Data, 5, 1, https://doi.org/10.3390/data5010001, 2019.

Matiu, M., Crespi, A., Bertoldi, G., Carmagnola, C. M., Marty, C., Morin, S., Schöner, W., Cat Berro, D., Chiogna, G., De Gregorio, L., Kotlarski, S., Majone, B., Resch, G., Terzago, S., Valt, M., Beozzo, W., Cianfarra, P., Gouttevin, I., Marcolini, G., Notarnicola, C., Petitta, M., Scherrer, S. C., Strasser, U., Winkler, M., Zebisch, M., Cicogna, A., Cremonini, R., Debernardi, A., Faletto, M., Gaddo, M., Giovannini, L., Mercalli, L., Soubeyroux, J.-M., Sušnik, A., Trenti, A., Urbani, S., and Weilguni, V.: Observed snow depth trends in the European Alps: 1971 to 2019, The Cryosphere, 15, 1343–1382, https://doi.org/10.5194/tc-15-1343-2021, 2021.

McGuire, K. J., Klaus, J., and Jackson, C. R.: JAMES BUTTLE REVIEW: Interflow, subsurface stormflow and throughflow: A synthesis of field work and modelling, Hydrol. Proc., 38, e15263, https://doi.org/10.1002/hyp.15263, 2024.

Meier, A.: Hydrological insights into glacier melt discharge: A multi-method approach using isotopes in a small alpine environment above 1745 m a.s.l., Master's thesis, University of Bern, https://www.geography.unibe.ch/unibe/portal/fak_naturwis/e_geowiss/c_igeogr/content/e39592/e1608235/e1608239/pane1608241/e1611621/Meier.Anna_2024_komprimiert_ger.pdf (last access: 15 February 2026), 2024.

Michel, A., Schaefli, B., Wever, N., Zekollari, H., Lehning, M., and Huwald, H.: Future water temperature of rivers in Switzerland under climate change investigated with physics-based models, Hydrol. Earth Syst. Sci., 26, 1063–1087, https://doi.org/10.5194/hess-26-1063-2022, 2022.

Monteith, J.: Evaporation and surface temperature, Q. J. R. Meteorol. Soc., 107, 1–27, 1981.

Müller, T., Lane, S. N., and Schaefli, B.: Towards a hydrogeomorphological understanding of proglacial catchments: an assessment of groundwater storage and release in an Alpine catchment, Hydrol. Earth Syst. Sci., 26, 6029–6054, https://doi.org/10.5194/hess-26-6029-2022, 2022.

Müller, T., Roncoroni, M., Mancini, D., Lane, S. N., and Schaefli, B.: Current and future roles of meltwater–groundwater dynamics in a proglacial Alpine outwash plain, Hydrol. Earth Syst. Sci., 28, 735–759, https://doi.org/10.5194/hess-28-735-2024, 2024.

Nan, Y., Tian, L., He, Z., Tian, F., and Shao, L.: The value of water isotope data on improving process understanding in a glacierized catchment on the Tibetan Plateau, Hydrol. Earth Syst. Sci., 25, 3653–3673, https://doi.org/10.5194/hess-25-3653-2021, 2021.

Nan, Y., Tian, F., McDonnell, J., Ni, G., Tian, L., Li, Z., Yan, D., Xia, X., Wang, T., Han, S., and Li, K.: Glacier meltwater has limited contributions to the total runoff in the major rivers draining the Tibetan Plateau, npj Clim. Atmos. Sci., 8, 155, https://doi.org/10.1038/s41612-025-01060-6, 2025.

Nash, J. E. and Sutcliffe, J. V.: River flow forecasting through conceptual models part I – a discussion of principles, J. Hydrol., 10, 282–290, 1970.

Owen, L. A. and Dortch, J. M.: Nature and timing of Quaternary glaciation in the Himalayan–Tibetan orogen, Quat. Sci. Rev., 88, 14–54, https://doi.org/10.1016/j.quascirev.2013.11.016, 2014.

Paillex, A., Siebers, A. R., Ebi, C., Mesman, J., and Robinson, C. T.: High stream intermittency in an alpine fluvial net-

work: Val Roseg, Switzerland, Limnol. Oceanogr., 65, 557–568, https://doi.org/10.1002/lno.11324, 2020.

Paschalis, A., Bonetti, S., Guo, Y., and Fatichi, S.: On the uncertainty induced by pedotransfer functions in terrestrial biosphere modeling, Water Resour. Res., 58, e2021WR031871, https://doi.org/10.1029/2021WR031871, 2022.

Pistocchi, A.: Simple estimation of snow density in an Alpine region, J. Hydrol. Reg. Stud., 6, 82–89, https://doi.org/10.1016/j.ejrh.2016.03.004, 2016.

Pomeroy, J., Gray, D., Brown, T., Hedstrom, N., Quinton, W., Granger, R., and Carey, S.: The cold regions hydrological model: a platform for basing process representation and model structure on physical evidence, Hydrol. Proc., 21, 2650–2667, https://doi.org/10.1002/hyp.6787, 2007.

Pourali, S., Arrowsmith, C., Chrisman, N., Matkan, A., and Mitchell, D.: Topography wetness index application in flood-risk-based land use planning, Appl. Spat. Anal. Policy, 9, 39–54, https://doi.org/10.1007/s12061-014-9130-2, 2016.

Puspitarini, H. D., François, B., Zaramella, M., Brown, C., and Borga, M.: The impact of glacier shrinkage on energy production from hydropower-solar complementarity in alpine river basins, Sci. Tot. Environ., 719, 137488, https://doi.org/10.1016/j.scitotenv.2020.137488, 2020.

Ramskogler, K., Knoflach, B., Elsner, B., Erschbamer, B., Haas, F., Heckmann, T., Hofmeister, F., Piermattei, L., Ressl, C., Trautmann, S., Wimmer, M. H., Geitner, C., Stötter, J., and Tasser, E.: Primary succession and its driving variables – a sphere-spanning approach applied in proglacial areas in the upper Martell Valley (Eastern Italian Alps), Biogeosciences, 20, 2919–2939, https://doi.org/10.5194/bg-20-2919-2023, 2023.

Reato, A., Borzi, G., Martínez, O. A., and Carol, E.: Role of rock glaciers and other high-altitude depositional units in the hydrology of the mountain watersheds of the Northern Patagonian Andes, Sci. Tot. Environ., 824, 153968, https://doi.org/10.1016/j.scitotenv.2022.153968, 2022.

Rehfeldt, K. R., Boggs, J. M., and Gelhar, L. W.: Field study of dispersion in a heterogeneous aquifer: 3. Geostatistical analysis of hydraulic conductivity, Water Resour. Res., 28, 3309–3324, https://doi.org/10.1029/92WR01758, 1992.

Richards, L. A.: Capillary conduction of liquids through porous mediums, Physics, 1, 318–333, https://doi.org/10.1063/1.1745010, 1931.

Riihimäki, H., Kemppinen, J., Kopecký, M., and Luoto, M.: Topographic Wetness Index as a proxy for soil moisture: The importance of flow-routing algorithm and grid resolution, Water Resour. Res., 57, e2021WR029871, https://doi.org/10.1029/2021WR029871, 2021.

Rinderer, M., van Meerveld, H. J., and Seibert, J.: Topographic controls on shallow groundwater levels in a steep, prealpine catchment: When are the TWI assumptions valid?, Water Resour. Res., 50, 6067–6080, https://doi.org/10.1002/2013WR015009, 2014.

Rounce, D. R., Hock, R., Maussion, F., Hugonnet, R., Kochtitzky, W., Huss, M., Berthier, E., Brinkerhoff, D., Compagno, L., Copland, L., Farinotti, D., Menounos, B., and McNabb, R.: Global glacier change in the 21st century: Every increase in temperature matters, Science, 379, 78–83, https://doi.org/10.1126/science.abo1324, 2023.

Schaefli, B. and Huss, M.: Integrating point glacier mass balance observations into hydrologic model identification, Hydrol. Earth Syst. Sci., 15, 1227–1241, https://doi.org/10.5194/hess-15-1227-2011, 2011.

Schaefli, B., Nicótina, L., Imfeld, C., Da Ronco, P., Bertuzzo, E., and Rinaldo, A.: SEHR-ECHO v1.0: a Spatially Explicit Hydrologic Response model for ecohydrologic applications, Geosci. Model Dev., 7, 2733–2746, https://doi.org/10.5194/gmd-7-2733-2014, 2014.

Schaffhauser, T., Tuo, Y., Hofmeister, F., Chiogna, G., Huang, J., Merk, F., and Disse, M.: SWAT-GL: A new glacier routine for the hydrological model SWAT, J. Am. Water Resour. Assoc., 60, 755–766, https://doi.org/10.1111/1752-1688.13199, 2024.

Schlögl, S., Marty, C., Bavay, M., and Lehning, M.: Sensitivity of Alpine3D modeled snow cover to modifications in DEM resolution, station coverage and meteorological input quantities, Environ. Model. Softw., 83, 387–396, https://doi.org/10.1016/j.envsoft.2016.02.017, 2016.

Schmid, E.: High alpine winter discharge development in Switzerland, Zenodo [data set], https://doi.org/10.5281/zenodo.13685009, 2024.

Schulla, J.: Hydrologische Modellierung von Flussgebieten zur Abschätzung der Folgen von Klimaänderungen, Eidgenössische technische Hochschule Zürich, Zürich, 189 pp., https://www.wasim.ch/downloads/doku/wasim/schulla_1997.pdf (last access: 15 February 2024), 1997.

Schulla, J.: Model Description WaSiM (Water balance Simulation Model), http://www.wasim.ch/downloads/doku/wasim/wasim_2024_en.pdf (last access: 15 February 2024), 2024.

Seibert, J. and Bergström, S.: A retrospective on hydrological catchment modelling based on half a century with the HBV model, Hydrol. Earth Syst. Sci., 26, 1371–1388, https://doi.org/10.5194/hess-26-1371-2022, 2022.

Sen, P.: Estimates of the regression coefficient based on Kendall's τ, J. Am. Stat. Assoc., 63, 1379–1389, https://doi.org/10.1080/01621459.1968.10480934, 1968.

Shrestha, M., Wang, L., Koike, T., Tsutsui, H., Xue, Y., and Hirabayashi, Y.: Correcting basin-scale snowfall in a mountainous basin using a distributed snowmelt model and remote-sensing data, Hydrol. Earth Syst. Sci., 18, 747–761, https://doi.org/10.5194/hess-18-747-2014, 2014.

Somers, L. D. and McKenzie, J. M.: A review of groundwater in high mountain environments, Wiley Interdisciplinary Reviews: Water, 7, e1475, https://doi.org/10.1002/wat2.1475, 2020.

Somers, L. D., Gordon, R. P., McKenzie, J. M., Lautz, L. K., Wigmore, O., Glose, A., Glas, R., Aubry-Wake, C., Mark, B., Baraer, M., and Condom, T.: Quantifying groundwater–surface water interactions in a proglacial valley, Cordillera Blanca, Peru, Hydrol. Proc., 30, 2915–2929, https://doi.org/10.1002/hyp.10912, 2016.

Stutenbecker, L., Costa, A., and Schlunegger, F.: Lithological control on the landscape form of the upper Rhône Basin, Central Swiss Alps, Earth Surf. Dyn., 4, 253–272, https://doi.org/10.5194/esurf-4-253-2016, 2016.

Talbot, F., Sylvain, J.-D., Drolet, G., Poulin, A., and Arsenault, R.: Enhancing physically based and distributed hydrological model calibration through internal state variable constraints, EGUsphere [preprint], https://doi.org/10.5194/egusphere-2024-3353, 2024.

Thornton, J. M., Brauchli, T., Mariethoz, G., and Brunner, P.: Efficient multi-objective calibration and uncertainty analysis of distributed snow simulations in rugged alpine terrain, J. Hydrol.,

598, 126241, https://doi.org/10.1016/j.jhydrol.2021.126241, 2021.

Thornton, J. M., Therrien, R., Mariéthoz, G., Linde, N., and Brunner, P.: Simulating fully-integrated hydrological dynamics in complex alpine headwaters: potential and challenges, Water Resour. Res., 58, e2020WR029 390, https://doi.org/10.1029/2020WR029390, 2022.

Trancoso, R., Larsen, J. R., McAlpine, C., McVicar, T. R., and Phinn, S.: Linking the Budyko framework and the Dunne diagram, J. Hydrol., 535, 581–597, https://doi.org/10.1016/j.jhydrol.2016.02.017, 2016.

Trinh, T., Kavvas, M., Ishida, K., Ercan, A., Chen, Z., Anderson, M., Ho, C., and Nguyen, T.: Integrating global land-cover and soil datasets to update saturated hydraulic conductivity parameterization in hydrologic modeling, Sci. Tot. Environ., 631, 279–288, https://doi.org/10.1016/j.scitotenv.2018.02.267, 2018.

Tuo, Y., Marcolini, G., Disse, M., and Chiogna, G.: A multi-objective approach to improve SWAT model calibration in alpine catchments, J. Hydrol., 559, 347–360, https://doi.org/10.1016/j.jhydrol.2018.02.055, 2018.

van Tiel, M., Aubry-Wake, C., Somers, L., Andermann, C., Avanzi, F., Baraer, M., Chiogna, G., Daigre, C., Das, S., Drenkhan, F., Farinotti, D., Fyffe, C., de Graaf, I., Hanus, S., Immerzeel, W., Koch, F., McKenzie, J., Müller, T., Popp, A., Saidaliyeva, Z., Schaefli, B., Schilling, O., Teagai, K., Thornton, J., and Yapiyev, V.: Cryosphere–groundwater connectivity is a missing link in the mountain water cycle, Nature Water, pp. 1–14, https://doi.org/10.1038/s44221-024-00277-8, 2024.

Voigt, C., Schulz, K., Koch, F., Wetzel, K.-F., Timmen, L., Rehm, T., Pflug, H., Stolarczuk, N., Förste, C., and Flechtner, F.: Technical note: Introduction of a superconducting gravimeter as novel hydrological sensor for the Alpine research catchment Zugspitze, Hydrol. Earth Syst. Sci., 25, 5047–5064, https://doi.org/10.5194/hess-25-5047-2021, 2021.

Warscher, M., Strasser, U., Kraller, G., Marke, T., Franz, H., and Kunstmann, H.: Performance of complex snow cover descriptions in a distributed hydrological model system: A case study for the high Alpine terrain of the Berchtesgaden Alps, Water Resour. Res., 49, 2619–2637, https://doi.org/10.1002/wrcr.20219, 20, 2013.

Wechsler, T., Stähli, M., Jorde, K., Zappa, M., and Schaefli, B.: The future of Alpine Run-of-River hydropower production: Climate change, environmental flow requirements, and technical production potential, Sci. Tot. Environ., 890, 163934, https://doi.org/10.1016/j.scitotenv.2023.163934, 2023.

Welch, R. M. and Shaw, J. H.: Structural styles and kinematic evolution of the Front Ranges of the Southern Canadian Rockies, Geosphere, 21, 605–636, https://doi.org/10.1130/GES02814.1, 2025.

Winkler, M., Schellander, H., and Gruber, S.: Snow water equivalents exclusively from snow depths and their temporal changes: the △snow model, Hydrol. Earth Syst. Sci., 25, 1165–1187, https://doi.org/10.5194/hess-25-1165-2021, 2021.

Woodbury, A. D. and Sudicky, E. A.: The geostatistical characteristics of the Borden aquifer, Water Resour. Res., 27, 533–546, https://doi.org/10.1029/90WR02545, 1991.

Xiang, L., Wang, H., Steffen, H., Wu, P., Jia, L., Jiang, L., and Shen, Q.: Groundwater storage changes in the Tibetan Plateau and adjacent areas revealed from GRACE satellite gravity data, Earth Planet. Sci. Lett., 449, 228–239, https://doi.org/10.1016/j.epsl.2016.06.002, 2016.

Xie, S., Zeng, C., Zhang, F., Wang, G., and Xiao, X.: Defining lateral subsurface flow and identifying its water sources in an alpine-permafrost hillslope, Catena, 236, 107765, https://doi.org/10.1016/j.catena.2023.107765, 2024.

Zhang, Z., Gu, Z., Hu, K., Hu, K., Xu, Y., and Zhao, J.: Spatial variability between glacier mass balance and environmental factors in the High Mountain Asia, J. Arid Land, 14, 441–454, https://doi.org/10.1007/s40333-017-0014-z, 2022.